

# Dynamics of the Mediterranean droughts from 850 to 2099 AD in the Community Earth System Model

Woon Mi Kim<sup>1,2</sup> and Christoph C. Raible<sup>1,2</sup>

<sup>1</sup>Climate and Environmental Physics, University of Bern, Switzerland

<sup>2</sup>Oeschger Centre for Climate Change Research, University of Bern, Switzerland

**Correspondence:** Woon Mi Kim (woonmi.kim@climate.unibe.ch)

## Abstract.

In this study, we analyze the dynamics of multi-year long droughts over the western and central Mediterranean region for the period of 850 - 2099 AD using the Community Earth System model version 1.0.1. Our study indicates that Mediterranean droughts during the period of 850 - 1849 AD are mainly driven by the internal variability of the climate system. A barotropic high pressure system together with a positive temperature anomaly over central Europe and the Mediterranean region is the prominent pattern that occurs in all seasons with droughts. Also, the modes of variability, i.e. the North Atlantic Oscillation (NAO) and El Niño Southern Oscillation (ENSO), are associated with Mediterranean multi-year droughts, showing that droughts occur more frequently with positive NAO and La Niña-like conditions. These modes of variability play a more dominant role during the initial stage of droughts. However, their role diminishes with the evolution of droughts, and after the initial stage, the persistence of multi-year droughts is determined by the interaction between the regional atmospheric and soil moisture variables. This atmosphere – soil interaction becomes stronger during the 1850 – 2099 AD period, reducing the importance of modes of variability on droughts and inducing a constant dryness over the Mediterranean region. Additionally, the discrepancy among diverse drought metrics in representing duration and frequencies of past droughts is presented, re-affirming the necessity of assessing a variety of drought indices even in the paleoclimate context.

## 15 1 Introduction

Drought is an extreme weather and climate event characterized by a prolonged period with persistent depletion of atmospheric moisture and surface water balance from its mean average condition. Drought is also characterized by a slow onset and devastating impacts on society, the economy and the environment (Wilhite, 1993; Dai, 2011; Mishra and Singh, 2010), and it can be classified in four types: meteorological drought, associated with the decrease in precipitation; agricultural drought, associated with the depletion of soil moisture and impacts on crops and plants; hydrological drought, characterized by the depletion of streamflow and water reservoirs, and lastly socio-economic drought, that occurs when the other types of droughts cause impacts on society, in a way that the water supply cannot meet the demand from society (Mishra and Singh, 2010). If a drought lasts for a longer time period, meteorological drought is transformed to other kind of droughts, agricultural and/or hydrological, and different types of droughts become interconnected to each other (Wang et al., 2016; Zhu et al., 2019). The severity

25 and duration of a drought can be quantified through different indices that capture hydrological conditions associated with a regional water balance (Dai, 2011). However, a single universal index cannot characterize the entire complexity of the nature of droughts (Lloyd-Hughes, 2014) and interconnection among different types of droughts (Mukherjee et al., 2018). Thus, one index does not necessarily produce a value that is similar to other indices even for the same region and period (Raible et al., 2017; Mukherjee et al., 2018). Some of the widely used indices are the self-calibrated Palmer Drought Severity Index (Wells et al., 2004), the Standardized Precipitation Index (McKee et al., 1993), and the Standardized Precipitation Evapotranspiration Index (Vicente-Serrano et al., 2009), among many others.

The Mediterranean region is known as a climate change hot-spot (Giorgi, 2006), meaning that the region is one of the most responsive to the current and future global warming, mainly associated with the decrease in precipitation and increase in drought episodes (Dubrovský et al., 2014; Liu et al., 2018). The climate of the Mediterranean is characterized as semi-arid with a pronounced annual cycle, thus, high temporal and spatial variability of the availability of water resources (Lionello et al., 2006). Therefore, droughts or periods with scarcity of water are intrinsic parts of the climatic conditions over Mediterranean. Overall, the region shows mild and wet winters, and hot and dry summers (Lionello et al., 2006). The variability of precipitation is not uniform across the entire Mediterranean area. The western and eastern regions show different precipitation regimes during the winter. A regional mode of circulation that explains a large percentage of the variability in winter is characterized by opposite pressure and precipitation patterns between the west-central and eastern Mediterranean regions, known as Mediterranean Oscillation (Dükeloh and Jacobeit, 2003). Besides, the regional precipitation is strongly influenced by the mid-latitude storm tracks and cyclones, which become stronger during the winter (Lionello et al., 2016; Raible et al., 2007, 2010; Ulbrich et al., 2009), regional cyclones (Alpert et al., 1990), and large-scale modes of variability, such as the North Atlantic Oscillation (NAO), East Atlantic - West Russian pattern (EA - WR) and El Niño-Southern Oscillation (ENSO) (Lionello et al., 2006; Raible, 2007). The influence of these large-scale patterns also varies within the region. The NAO exerts its control on precipitation by affecting the strength of westerlies and latitudinal movement of the storm tracks. This influence largely becomes stronger during the wintertime. The precipitation decreases during the positive NAO, mostly in the west-central Mediterranean region, and the opposite condition occurs during the negative NAO (Wallace and Gutzler, 1981; Hurrell, 1995). The influence of EA-WR in European hydroclimate is also stronger in the winter. During the positive (negative) phase, the southeastern Mediterranean region experiences drier (wetter) condition than on average (Barnston and Livezey, 1987; Krichak and Alpert, 2005). The response of the Mediterranean climate on ENSO is more complex and not straightforward: it varies over time, discussed for a few historical cases (Brönnimann, 2007; Brönnimann et al., 2007), it depends on the maturity of the ENSO state (Vicente-Serrano, 2005), on the seasons (Mariotti et al., 2002) and on the co-occurrence with NAO (Brönnimann, 2007; Raible et al., 2001, 2003). Mariotti et al. (2002) demonstrated that precipitation decreases over the western Mediterranean during La Niña in autumn and spring. Brönnimann (2007) showed a connection between La Niña (El Niño) and the positive (negative) phase of the NAO in the late winter.

In the Mediterranean region, the increases in the severity and number of droughts over the region have been already detected in the modern observational records since the mid to late 20th century through different drought indices (e.g., Mariotti et al., 2008; Philandras et al., 2011; Sousa et al., 2011; Seager et al., 2014; Vicente-Serrano et al., 2014; Spinoni et al., 2015).

60 Furthermore, in recent decades, the occurrence of droughts with pan-European characteristic that cover a large part of the west-  
central Mediterranean region have been detected (García-Herrera et al., 2019; Spinoni et al., 2017). The increase in dryness  
is attributed to the increase in the atmospheric greenhouse gases (GHG) concentration, which causes a strong increase in the  
surface temperature and decrease in precipitation over the region (Mariotti et al., 2008). General circulation models (GCMs)  
project that this drying trend together with the increases in dry days and drought episodes will be intensified in the future under  
65 the business-as-usual scenario, causing important socio-economic impacts and changes in the region (Mariotti et al., 2008;  
Field et al., 2012; Lehner et al., 2017; Naumann et al., 2018). The future changes in the Mediterranean droughts are due to the  
tropical SST warming (Hoerling et al., 2011), changes in mean regional circulation associated with intensified subsidence and  
low-level mass divergence (Seager et al., 2014), expansion of the Hadley cell and the expansion of the subtropical subsidence  
zones (Previdi and Liepert, 2007), intensification of subtropical highs (Li et al., 2012), and northward shift of the storm tracks  
70 (Raible et al., 2010).

Though the dryness projected in the future scenarios by GCMs is unprecedentedly intense, multi-years long desiccation is  
not a completely new phenomenon over the Mediterranean area. Using the summer self-calibrated Palmer Drought Severity  
Index (scPDSI) based on tree rings (also known as the Old World Drought Atlas; OWDA; Cook et al. 2015), Cook et al.  
(2016a) showed that there have been several dry periods during the last 900 years over the region, some with persistent pan-  
75 Mediterranean characteristics. The region has experienced drought variability with frequencies of not only interannual, but  
multidecadal timescales. Although, the causes of those droughts in the past are still unclear, they show some connection with  
the large-scale patterns such as NAO, ER-WR and Scandinavian pattern.

Besides natural climate proxies, GCMs have been used to study long-term changes and continuous variability of global and  
regional hydroclimate and extreme events during the last millennium (PAGES Hydro2k Consortium, 2017; Haywood et al.,  
80 2019). Modelling studies on the long-term variability of droughts are focused on the U.S continent, mainly to investigate  
the continuous variability and mechanisms of South Western United States (SW) droughts, the Medieval Climate Anomaly  
(MCA) SW megadroughts, and North American pan-continental droughts (e.g., Coats et al., 2013, 2016; Coats and Karnauskas,  
2017; Cook et al., 2016b; Parsons et al., 2018; Parsons and Coats, 2019). The results show that different GCMs are able to  
reproduce the duration and intensity of SW megadroughts and North American pan-continental droughts, indicating the internal  
85 variability as the main driver, though specific causing modes of variability are largely model dependent. Parsons and Coats  
(2019) investigated the evolution of SW multi-year droughts and their associated modes of variability using the Community  
Earth System Last Millennium Ensemble (CESM-LME; Otto-Bliesner et al. 2016). Their study suggests that the connection  
between the Tropical Equatorial Pacific and SW droughts changes with the stage of multi-year droughts, showing that La Niña  
is more common during the initiation years, then, cool and neutral Tropical Pacific condition and tendency to El Niño increase  
90 in middle years. Previously, Namias (1960) also analyzed the evolution of droughts by associating different stages of droughts  
with the atmospheric circulation in the Northern Hemisphere.

Stevenson et al. (2018) used the CESM - LME to examine the connection between past global hydrological mega-events,  
and climate variability and external forcings during the last millennium. Among the major modes of climate variability, the  
influences of ENSO and AMO on mega-events have been found, both significantly altering the megadrought risks and per-

95 sistance in drought-prone regions, for instance, the southern Australia, the Sahel and the southern United States. The study provides insights into the dynamic of megadroughts associated with different mode of variability in global scale, though, a detailed analysis on southern Europe and the Mediterranean is missing.

In studies of the hydroclimate during last millennium over the European domain, Ljungqvist et al. (2019) examined a long-term covariability between the summer temperature and hydroclimate during the Common Era. By comparing the instrumental records, tree ring-based reconstructions, and model simulations, they found that a warm-dry relationship with multi-decadal variability is more dominant in the southern Europe. Though, all datasets share some common leading modes of covariability across different time frequencies, there are some discrepancies among instrumental records, proxies, and model. The proxies present a stronger positive temperature-hydroclimate relationship, while the model exhibits a stronger negative relationship than the instrumental records. Xoplaki et al. (2018) investigated the interaction between the past central and eastern Mediterranean societies and the hydroclimate conditions including droughts, by comparing the historical records, proxies and GCM simulations. Analyzing three particular historical periods, they concluded that the multidecadal variability of precipitation in the region is driven by internal dynamics of the climate system: large discrepancies between the model trajectories are detected. Therefore, no agreement in timing between models-proxies-historical records can be expected. Nevertheless, the models elucidate some possible explanations about the dynamics of extreme dry and wet events in some past periods.

110 Despite a number of studies on past hydrological variability, a long-term continuous perspective on the mechanisms of past extreme hydrological events, specifically of droughts over the Mediterranean during the last millennium is still not fully explored. As a long trend of dryness has already been detected in the instrumental era and is expected to intensify in the future scenario, it is necessary to provide a long-term picture on the variability and changes of past dry events and their mechanisms. Therefore, we aim to examine the physical mechanisms involved in yearly and multi-year long droughts during the Common Era (850 - 1849 AD) and historical, present and future periods (1850 - 2099 AD) over the west-central Mediterranean region. We choose this specific area, as this region has been affected by recent large scale droughts (García-Herrera et al., 2019; Spinoni et al., 2017), which can be seen as pan-west-central Mediterranean droughts. Moreover, the region shows coherent desiccation in the future scenario (Dubrovský et al., 2014). From now on, for simplicity, we refer to the west-central Mediterranean region in our study simply as the Mediterranean region. We focus on understanding the dynamics that induce past persistent pan-120 regional multi-year droughts, and whether the dynamics that induce droughts in the past will change in the historical and future periods with the anthropogenic increase in GHG.

For our purpose, we use the Community Earth System Model version 1.0.1 (CESM), which includes the active biogeochemical cycle and has the horizontal resolution of  $1.25^\circ \times 0.9^\circ$  (Lehner et al., 2015). The spatial resolution of the model is a clear advantage for our study on a relatively small confined area. The precipitation of the region is strongly influenced by extratropical cyclones and in general, GCMs have difficulties in reproducing the dynamics and precipitation associated with these meso-scale phenomena (Raible et al., 2007; Watterson, 2006). Nevertheless, these atmospheric dynamics and precipitation are better represented in GCMs with finer spatial resolution (Champion et al., 2011; Watterson, 2006). Hence, using a model that provides a seamless simulation for period 850 – 2099 AD guarantees an improved representation of precipitation related processes, thus, drought associated mechanisms over the region.

130 This paper is composed of the following sections: in section 2, we introduce the model and simulations, the hydrological variables given by the model, definition of droughts, drought indices, proxy and observation datasets and methods. In section 3, we present the results of our analysis: first, we compare the simulations, proxy reconstructions and observation to validate our model; second, we describe how the model depicts past droughts, whether the quantification of past droughts over the region is sensitive to the choice of drought metrics, and whether there is some possible association between the volcanic eruptions and  
135 droughts; third, we report the climate conditions associated with the past Mediterranean droughts and their connection with regional scale circulation and modes of variability, i.e. the NAO and ENSO; lastly, we discuss whether mechanisms that induce past droughts have changed in the historical and future periods. In section 4, we present a conclusion of our analysis.

## 2 Model description and methods

### 2.1 Description of the model and simulations

140 We use the Community Earth System model version 1.0.1 and its continuous transient simulation of 1250 years (850 - 2099 AD) where the 2005 – 2099 AD is run with the RCP 8.5 scenario, and control simulation of 400 years at perpetual 850 AD conditions (Lehner et al., 2015). In the simulations, the atmosphere has the horizontal resolution of  $1.25^\circ \times 0.9^\circ$  and 26 vertical layers, and the land has the same horizontal resolution as the atmosphere with 15 sub-surface layers. The ocean has the horizontal resolution of  $1.25^\circ \times 0.9^\circ$  with displaced pole grids with 60 ocean layers.

145 The control simulation uses constant forcing parameters set to the 850 AD values: the land use changes, the total solar irradiance in which the value is  $1360.228 \text{ W m}^{-2}$ , the GHG concentration, such as the  $\text{CO}_2$  of 279.3 ppm,  $\text{CH}_4$  of 674.5 ppb and the  $\text{N}_2\text{O}$  of 266.9 ppb. Unlike other forcings, the orbital parameters are set to 1990 AD conditions.

The transient simulation includes the active biogeochemical cycle and forcings, such as the land use changes, total solar irradiance, volcanic eruptions and greenhouse gases concentrations that vary over time (Schmidt et al., 2012). The GHG  
150 concentrations and land use changes vary little before 1850, showing pronounced changes and increases after that year. A more detailed overview of the forcings and initial set-up of the simulations is presented in Lehner et al. (2015).

### 2.2 Region of study, analysis and methods

The focus area of the study is the western and central Mediterranean region confined to  $15^\circ\text{W} - 28^\circ\text{E}$  and  $33^\circ - 45^\circ\text{N}$  (Fig. 1). The extent of the region is selected based on Empirical Orthogonal Function analysis on the monthly precipitation from the  
155 observation (gridded station precipitation from U.Delaware v5.01; Willmott and Matsuura 2001). The region shares overall a similar variability in the first EOF (13.28%) and second EOF (11.01%), in which this similarity also can be attributed to the influence of North Atlantic Oscillation in precipitation over the region (Dünkeloh and Jacobeit, 2003).

For the analysis, the monthly anomalies of the variables associated with the hydrological condition, such as the surface and air temperatures, precipitation, zonal and meridional winds, geopotential heights, and sea level pressure are calculated with

160 respect to the 1000-1849 AD (850 years) mean annual cycle for each grid point in the transient simulation. For the control simulation, the entire 400 years are taken as a reference period to calculate the anomalies.

We split the transient simulation into two parts: the first period from 850 to 1849 AD is used to study the natural variability of droughts excluding the effect of accelerated increase in the GHGs, and the second period from 1850 to 2099 AD is used to examine the effects of anthropogenic changes on the natural variability of droughts.

165 The drought condition during the first period (850 – 1849 AD) is compared to the control simulation to assess the influence of the natural variability and forcings. The statistical tests to compare the transient to the control simulations are performed with the Mann-Whitney U significance test for the means at a 5% confidence level. First, the test is performed without considering the difference in the length of each simulation. Then, as the transient simulation is longer than the control one, we select 5 sets of random 89 years with droughts from the transient simulation and apply the tests against the control simulation.

170 For the second period (1850 - 2099 AD), the anomalies are linearly detrended in order to examine the background mechanisms associated with dryness during this period without the anthropogenic influence on climate. This is performed by splitting the time period into two and applying the least squares method to the each of the period separately: from 1850 to 2000 and from 2001 to 2099 AD. Then, the detrended anomalies are compared against the non-detrended anomalies for the same period and also for the first period.

175 Composites of positive and negative phases of two modes of variability are also investigated: the NAO and ENSO. The NAO is taken as the difference in the sea level pressure anomalies between the regions confined to  $33^{\circ} - 21^{\circ}\text{W} / 35^{\circ} - 39^{\circ}\text{N}$  and  $25^{\circ} - 13^{\circ}\text{W} / 63^{\circ} - 67^{\circ}\text{N}$ , which reflects the Azores high and the Iceland low respectively (Wallace and Gutzler, 1981; Trigo et al., 2002). The ENSO is characterized by the annual mean sea surface temperature anomalies over Niño 3.4 region in the Tropical Equatorial Pacific ( $170^{\circ} - 120^{\circ}\text{W}$  and  $5^{\circ}\text{S} - 5^{\circ}\text{N}$ ) (Trenberth, 1997).

180 We further perform wavelet coherence analysis (Grinsted et al., 2004; Gouhier et al., 2018) in order to find a possible time-varying association between droughts and volcanic eruptions, using the time series of volcanic eruptions (Gao et al., 2008) and of drought indices (Sect. 2.3). The time series are normalized to have a zero mean and one standard deviation.

### 2.3 Drought definitions

We use some drought metrics to quantify droughts and to perform the comparison among them: the Standardized Precipitation Index (SPI), Standardized Precipitation Evapotranspiration Index (SPEI), self-calibrated Palmer Drought Severity Index (scPDSI), and annual soil moisture anomaly (SOIL).

190 The SPI only requires a long-term precipitation record, and the accumulated precipitation is fitted to a probabilistic distribution, in our case a gamma distribution. Then, the fitted distribution is transformed to a normalized Gaussian distribution (McKee et al., 1993). The SPEI is similar to the SPI, but instead of only using a precipitation record, it considers the climate water balance given by the difference between the precipitation and atmospheric evaporative demand. This difference is fitted to a log-logistic probability distribution, then, transformed to a normal distribution (Vicente-Serrano et al., 2009). For the atmospheric evaporative demands, we use the potential evapotranspiration derived from Thornthwaite equation, which only requires surface temperature and latitude (Thornthwaite et al., 1948). The scPDSI computes the water balance by assuming a

two-layer soil bucket model, and it requires temperature and potential evapotranspiration records. Other necessary variables, such as runoff and losses, are estimated from the temperature and potential evapotranspiration (Palmer, 1965; Wells et al., 2004; Zhong et al., 2018). Again, the potential evapotranspiration is calculated by using Thornthwaite equation same as the SPEI. The SOIL is the upper 10 cm soil moisture anomaly calculated with respect to the 850 years-mean (1000-1849 AD) annual cycles. The soil moisture is a direct output from the model.

All indices are calculated with respect to the same reference period (1000-1849 AD), and with the 12 months-annual time scale for the SPI, SPEI and SOIL. The scPDSI has an inherent time scale that ranges from 9 to 14 months depending on the region (Vicente-Serrano et al., 2010, 2015). Thus, we use a 12 month-time scale for the other indices in order to be comparable to the scPDSI. Then, all indices are area weighted averaged over the Mediterranean region (Fig. 1). The summer scPDSI is also calculated by averaging the June-July-August scPDSI, in order to compare with the summer scPDSI from the tree ring-based reconstruction, the Old World Drought Atlas (OWDA; Cook et al. 2015).

For all indices, we define a drought event as consecutive years with negative indices, in which at least one year with the index falling below the 10 percentiles of its 850-year (1000 - 1849 AD) distribution. In such way, we assure that the dry condition is maintained consistently during drought years, without being interrupted by one wet year or season. This method that imposes a threshold based on the extreme percentiles, assures that strong negative anomalies persist throughout the entire year with droughts, thus, we only take relatively severe droughts for our analysis.

Droughts with a duration of more than 3 years are considered as multi-year droughts. In the Sect. 3.3., we analyze the mean condition during droughts in the control and transient simulations taking into account all short (1 and 2 years of duration) and long (more than 3 years of duration) Mediterranean droughts. For the next part of the analysis in the Sect. 3.4., we examine the dynamics associated with persistent multi-year droughts (more than 3 years of duration). These long droughts are separated into three stages: the initiation years as the first years of droughts, the termination years as the last years, and the rest as the transition years. The evolution of droughts is analyzed for each of the stages. This separation method is similar to the one used by Parsons and Coats (2019).

Lastly, in order to define droughts with pan-west-central Mediterranean characteristic, we select only drought events where more than 70% of the region of study is occupied by negative indices (Fig. 1.(b)). Though, for multi-year droughts, we allow that this condition does not need to be fulfilled for the initiation and termination years but only for the transition years: a drought can start weak and with a more local characteristic, then expand to a larger proportion of the Mediterranean, and weaken again in the termination years.

## 2.4 Observation and proxy reconstruction datasets

For the validation of the model, we compare mean seasonal precipitation and mean climate conditions associated with droughts among the observation, proxy reconstruction and model for the period of 1901 – 2000 AD. We use the gridded station data for temperature and precipitation from U.Delaware v5.01 (Willmott and Matsuura, 2001), the sea surface temperature from the Extended Reconstructed Sea Surface Temperature v5 (ERSST v5; Huang et al. 2017), and geopotential heights from the 21th Century Reanalysis v2 (CR v2; Compo et al. 2011). The scPDSI is calculated using the U.Delaware v5.01 temperature and

precipitation. Furthermore, we take the gridded tree-ring-based reconstruction of European summer scPDSI, OWDA (Cook et al., 2015). The analysis on drought associated patterns is performed using the spatial correlation analysis between the monthly scPDSI and SST, scPDSI and geopotential heights. Among all drought indices, we use only scPDSI for comparison and validation, as the OWDA only provides this specific drought metric. The anomalies of variables are calculated by extracting the mean annual cycles with respect to 1950 – 1979 AD. To calculate the scPDSI for the observation and model, the same period is used as the calibration period.

### 3 Results

#### 3.1 Validation of CESM: comparison among observation, proxy and model (1901 – 2000 AD)

In this section, we compare the mean precipitation, mean scPDSI, number and duration of droughts and atmospheric conditions associated with Mediterranean dry conditions among the observation, OWDA and CESM simulation for the period of 1901 – 2000 AD.

The Fig. 2 shows that the model exhibits similar spatial patterns of mean seasonal precipitation to those from the observation. Though, there are some regions where the seasonal means between the observation and model are statistically different. In the summer, both central and western Mediterranean present dry conditions, whereas in the winter, both regions are less dry than the summer with wet conditions over Portugal and Balkans. For the mean annual cycle, the model in general shows less precipitation than the observed values over both central and western Mediterranean. Nevertheless, the model reproduces well the annual precipitation cycle, depicting correctly the maximum and minimum periods of precipitation.

In terms of the droughts (Fig. 3.(a)), the means from the summer scPDSI between the model and OWDA are statistically similar to each other (p-value from the t-student test of 0.28). This is also the case between the OWDA and observation but with much lower confidence level of 1% (p value of 0.01). However, both summer and annual scPDSI from the model are statistically different to those from the observation (p-values of 0.001). In terms of the number of droughts (Fig. 3.(b)), the observation presents 4, OWDA 7 and CESM 3 events during the last century. For the duration of droughts, the mean (5.43 years) and median (3 years) from OWDA are different to those from the observation (11.50 and 12.50 years respectively), with OWDA exhibiting lower values. CESM also presents a lower median in the duration of droughts (6 years) compared to the observation, though, its mean (9.67 years) resembles better the observation than the one from OWDA. The discrepancies in the means and medians of droughts between the observation and CESM are still present in annual droughts.

We observe that the model tends to underestimate the duration of present-day droughts than those from the observation. However, the model still shows to a certain extent its ability to reproduce persistent long droughts, simulating droughts of few years long, and with longer duration than those from OWDA. Still, the analysis on annual-scale extreme dry events based on a relatively short present period of 100 years is not sufficient to draw comprehensive conclusions of present-day multi-years droughts, due to the limited number of events.

One of the reason for the difference in the overall scPDSI between the model and observation is potentially related to the model performance on meso-scale phenomena, which play an important role for the regional precipitation during the wet

season (Alpert et al., 1990; Ulbrich et al., 2009; Champion et al., 2011; Watterson, 2006). Additionally, the model performance on internal variability may contribute to this discrepancy, which will be discussed in the following paragraphs. The same can also explain the case of OWDA and observation, that shows a p-value at the limit of 1% confidence level. The annually resolved OWDA is based on tree rings, which are known to be biased towards the growing season, so that the full annual signal might  
265 be not fully preserved in such a reconstruction. Moreover, proxy model observation comparison studies show that tree ring-based reconstructions tend to deviate in their spectral behavior (Franke et al., 2013), and the distribution of tree rings used to generate the gridded reconstruction over Mediterranean (Cook et al., 2015) may not be enough to capture precipitation events associated with regional-scale cyclones and to fully explain dry/wet variability for the entire region (Babst et al., 2018).

After all, the model and observation share many common patterns associated with the scPDSI. The ocean and atmospheric  
270 condition associated with the variability of scPDSI in the observation and model are presented in Fig. (4) through the correlation patterns between the scPDSI and SST, and the scPDSI and geopotential height at 850hPa. The observation and model exhibit significant positive correlations over the central Equatorial Pacific, though in the observation, the region with statistically significant correlation is located more on the north-central Pacific than in the model. The observation and model share a significant wave-like pattern over the extratropical latitudinal belt, that extends from the North Pacific to Siberia. Within this  
275 wave-like pattern, a bipolar pattern with a significant negative correlation centered over Mediterranean region and a positive correlation over the northern high latitudes are prominent. In the observation, the area of negative correlation over Europe is larger and the positive correlation of the bipolar pattern is shifted more to the Scandinavian region than in the model. The observation and model present some common patterns occurring over the regions of ENSO and NAO.

It is known that the variability of ENSO is too strongly represented in CESM (Parsons et al., 2017; Stevenson et al., 2018).  
280 Nevertheless, the model is able to capture relatively well the hydroclimate condition associated with the ENSO teleconnection (Stevenson et al., 2018). In case of NAO, the seasonal variability of NAO seems to be amplified in many CMIP models (Fasullo et al., 2020). The CESM, however, resembles the present-day NAO pattern well and the spatial precipitation and temperature associated with this mode of variability in Europe (Deser et al., 2017). These inherent biases with respect to modes of variability (in particular for ENSO) can partially explain the differences we observe here between the model and observation.

285 Overall, the model is able to reproduce the climate condition associated with the variability of present-day scPDSI, despite the fact presents some discrepancy to the observation exist. Moreover, the model does not significantly underestimate the persistence of multi-year droughts. As it also shows statistical similarity to OWDA over the region, we consider that the model can be used for the analysis on past Mediterranean droughts. We take into account these differences of model to the observation and biases on modes of variability to discuss the implications of them in our results more in detail in the Sect. 4.

### 290 **3.2 Variability of Mediterranean droughts during the 850 - 1849 AD and their connection to the volcanic forcing**

To gain an overview of drought conditions in the Mediterranean, we assess the indices defined in the Sect. 2.3 using the period 850 to 1849 AD and focusing on the drought events and their duration. In the beginning, we compare the variability and duration of droughts of the summertime scPDSI from CESM with those from OWDA. We do not aim to make a direct comparison between the proxies and the model simulation, as this cannot be made due to the different initial conditions

295 between the proxies and model (PAGES Hydro2k Consortium, 2017; Xoplaki et al., 2018). Here, we rather focus on comparing the simulated summer drought variability with the one of the OWDA. Additionally, we assess whether the simulated and reconstructed droughts respond similarly to the same external forcing, i.e. the volcanic eruptions.

The Fig. 5.(a) and (c) exhibits the distribution and the 100 years running mean of duration of summer (June-July-August mean) in OWDA and CESM. In terms of duration of summer droughts (Fig. 5.(a)), the discrepancy between CESM and OWDA is clear, with OWDA presenting the mean duration of 5.38 years and CESM with 7.89 years. These means are statistically different to each other. This seems to be consistent with the result in the previous section (Sect. 3.1) that shows that OWDA has droughts with shorter duration compared to the present-day observation and CESM over the Mediterranean region. Thus, this characteristic is still present during the entire last millennium. The variability of droughts over time in OWDA and CESM is also different to each other (Fig. 5.(c)), without a specific common period of increase in droughts. This gives us a first hint that the occurrence of droughts over the region are not mainly driven by the external natural forcings. Both time series present a common period of decrease in droughts around 1600 AD.

Similarly, the Fig. 5.(b) and (d) show the distributions and running means of duration of annual Mediterranean droughts in CESM quantified using different indices. As expected, different indices do not exactly behave similarly in terms of the occurrence, number of events, and duration (Raible et al., 2017; Mukherjee et al., 2018). However, the indices coincide for some years: in total 89 years of the 850 - 1849 AD period, all indices indicate the same overlapped drought periods. In terms of duration, the scPDSI is the one which shows more longer lasting droughts than other indices, with a mean duration of 9.1 years. Then, the SPEI, SOIL and SPI follow it with the mean durations of 2.9, 2.8, and 2.3 years, respectively. The SPI presents more events than other indices, but with shorter duration. All these means are statistically different among each other, except the means between SPEI and SOIL, which are statistically indifferent (p-value of 0.87).

The difference in duration of droughts among indices can be attributed to the water balance variables involved in the computation of each index. For instance, the SPI only takes precipitation as its input variable. Thus, it does not consider the atmospheric evaporative demands, which can be intensified during dry periods. Therefore, we expect that the SPI shows a reduced duration of droughts compared to the scPDSI and SPEI, which include the potential evapotranspiration in their water balance. The same holds true for the SOIL index. Though, the soil moisture in the model is closely connected to the hydrological cycle reflecting the balance between the precipitation and actual evapotranspiration, the magnitude of actual evapotranspiration over the region is smaller than the potential evapotranspiration derived from the Thornthwaite method. Hence, the water balance involved in SOIL is affected in such a way that the drought duration is reduced compared to the scPDSI and SPEI. Lastly, droughts with relatively longer duration in the scPDSI can be explained by the memory effect embedded in the calculation scheme of scPDSI (Palmer, 1965; Wells et al., 2004), which other indices that are obtained by being normalized with respect to certain statistical distribution families do not present. The scPDSI is an accumulating index; therefore, during the calculation process, the weighted value of preceding months is used to estimate the index for the current month, implying a persistence of the events. Hence, with the scPDSI, an intense yearly drought would likely induce a drought in the following year and this effect can be exacerbated in the context of intense multi-year droughts.

In terms of variability over the period of 850 - 1849 AD (Fig. 5.(d)), at first glance, similarly to the summertime OWDA and CESM, no noticeable coherent changes among all indices, such as a common period of increase in the occurrence of droughts over time, is noticed. Although each index captures slightly different aspects of water balance, we expect to see a similar common response to external forcing among all the indices, if droughts are influenced by the same externally forced variability, e.g., the volcanic forcing. However, this is not the case. The wavelet coherence analysis between the drought indices and volcanic eruptions corroborates the absence of a connection between these two variables (Fig. 6). The signals of statistically significant coherent variability between drought indices (SOIL and scPDSI) in CESM and volcanic eruptions are not uniform across the period-year frequency bands. Before 1100 AD, the anti-phase relationship between the two variables dominates, while after 1100 AD is the opposite, an in-phase relationship is more visible. Moreover, the leading variables of association also change over the time and frequency band. This is the same for OWDA. Besides, OWDA does not show strong significant signal during the 1257 Samala eruption, which was the strongest eruption in the last millennium (Gao et al., 2008). Hence, the analysis confirms that the occurrence of yearly and multi-year Mediterranean droughts are not driven by the volcanic eruptions, rather, the driver can be attributed to the internal variability.

In the next sections, we investigate the underlying dynamics using only the SOIL as the drought indicator in order to understand the role of the internal variability in Mediterranean droughts. The focus on one indicator is motivated by the fact that soil moisture reflects the regional hydrological balance associated with the precipitation and evapotranspiration, and it is also an indicative of water stress on plants and ecosystem (Berg et al., 2017; Swann, 2018). Another advantage of this index is that the variable is a direct output from the model, thus, it does not require any further step, except for calculating the anomalies, and statistical assumptions as other indices do. Moreover, using the SOIL helps us to avoid the overestimation of drought risk and severity that occurs with many offline drought indices. The offline estimation of droughts by some common drought metrics, such as scPDSI, tends to magnify the impact of increase in temperature, therefore in potential evapotranspiration, on drought-associated atmosphere - surface feedback (Seneviratne et al., 2010). Hence, in the warming scenario, the indices that are constructed based on atmospheric supply and demand of moisture, such as scPDSI and SPEI, strongly overestimate future drought risks (Berg et al., 2017; Cook et al., 2018; Swann et al., 2016).

In our analysis, the SOIL overlaps full or a part of drought periods given by the other three indices, without significantly underestimating the multi-year duration of droughts. The droughts in SOIL overlap the 36%, 25% and 29% of droughts in the scPDSI, SPEI and SPI, respectively. Also, the SOIL and each of the indices are statistically correlated at 1% confidence level for the entire period of 850 -1849 AD with Pearson correlation coefficients of 0.81 (thus, 66% of variance) with scPDSI, 0.78 (0.61%) with SPEI and 0.86 (74%) with SPI. Hence, the results in the following sections can be transferred to the other indices. To guarantee the transferability, the analysis in the next sections was repeated with each of the drought indices, showing similar results as for SOIL (therefore figures not shown).

### 360 3.3 Atmospheric circulation associated with Mediterranean droughts (850 - 1849 AD)

In this section, the atmospheric circulation associated with Mediterranean droughts is investigated by using the SOIL in the control and transient simulations up to 1849 AD. The control simulation presents 7.25 droughts every century, with the mean duration of 3.06 years and the transient simulation has 8 droughts every century with the mean duration of 2.81 years.

To get a first glance of the atmospheric circulation during drought conditions, Fig. 7 shows the anomalies of geopotential height at 850 hPa and surface temperature during Mediterranean droughts for each simulation. The structures of geopotential height and temperature anomalies during Mediterranean droughts are similar, with a high-pressure system centered over central Europe accompanied by a positive temperature anomaly. This high-pressure anomaly, which from now on is called the drought high, is found in all heights from the 850 to 300 hPa (figures not shown), indicating a barotropic nature of this atmospheric circulation system. Additionally, a low pressure anomaly is situated over the area of Scandinavia to Russia. Thus, the atmospheric circulation shows a north easterly shift of the westerlies over Europe, so that moist air masses from the North Atlantic are passed around the Mediterranean.

Outside the European continent, a negative temperature anomaly over the Tropical Equatorial Pacific and a positive anomaly over the North Pacific are prominent in both simulations. These temperature patterns resemble the cold phase of ENSO and the positive phase of Pacific Decadal Oscillation (PDO), respectively. Besides, a positive geopotential height anomaly at the mid-latitudes and a negative anomaly at the high latitudes over the North Atlantic region is another pattern that both simulations share in common during droughts. This pattern is similar to the positive phase of the NAO; however, the southerly center of action is shifted to central Europe, which also resembles partially the East Atlantic Pattern (EA). The means of these common patterns are also statistically indifferent between both simulations, indicating that they are derived from the same statistical populations. Thus, they share common mechanisms associated with droughts, mainly driven by the internal variability of the climate system in the model, embedded both in control and transient simulations.

The drought high is a clear feature that appears during all droughts over the region. This pattern over central Europe and the western Mediterranean is similar to the pattern of the first mode of canonical correlation described by Xoplaki et al. (2003). In Xoplaki et al. (2003), this pattern is associated with the variability of temperature during the summertime in the Mediterranean region. In our study, the high-pressure system is present during all seasons of years with droughts, showing a relatively stronger intensity in winter and spring compared to summer (Fig. 8). This is expected, as the variability of the geopotential height fields over Europe and the North Atlantic is reduced in summer compared to the other seasons, because the meridional temperature gradient on the Northern Hemisphere is also reduced. Therefore, the main forcing of the atmospheric circulation is weakened. Our findings show that the atmospheric conditions in wet seasons, i.e. winter and spring, are determinant at controlling the annual mean hydroclimate, thus, indicating the importance of precipitation and dynamics during the wet season in annual-scale Mediterranean droughts (Lionello et al., 2006; Xoplaki et al., 2004; Zveryaev, 2004).

As expected, a decrease in precipitation occurs in all seasons during droughts: the winter and spring precipitation decreases by around 13%, and the summer and autumn precipitation by 11% compared to non-drought periods. These changes in precipitation are in the range of the rates of expected decrease in annual precipitation over the Mediterranean region in the future

scenario. In the future, the regional precipitation is expected to reduce by 5 – 30% from its present-day value and this will cause  
395 water shortage related issues in the region (Dubrovský et al., 2014; Mariotti et al., 2008). The temperature shows a positive  
anomaly over the region in all seasons, with strongest signals during summer and autumn, a finding which is in line with, e.g.,  
Xoplaki et al. (2003). This indicates that Mediterranean droughts are more associated with anomalously warmer atmospheric  
conditions.

### 3.4 Dynamics of multi-year droughts

400 For the analysis on multi-years Mediterranean droughts, among all drought events, we take only droughts with a minimum  
duration of 3 years. As shown in the previous section in Fig. 7, the drought high is a prominent atmospheric circulation pattern  
with the negative geopotential height anomaly north-east to it. The entire pattern resembles the positive NAO-like pattern,  
although with a shift to the North-East. At the same time, a colder than normal condition over the Tropical Equatorial Pacific  
is detected, which is similar to a La Niña-like condition. In the following, we investigate the origin and the evolution of  
405 Mediterranean long droughts associated to NAO, ENSO-like condition and drought high using the transient simulation up to  
1849 AD.

The phases of NAO and ENSO are defined with respect to the non-drought periods: the values below 25 (above 75) percentile  
of NAO and ENSO during the non-droughts periods are considered as negative (positive) phases of NAO and ENSO respec-  
tively (Fig. 9). For the co-occurrence of droughts and the positive phase of NAO, the simulation shows that droughts occur  
410 more frequently during the positive phase of annual and winter NAO than during normal years without droughts: 38% of the  
drought years show the positive phase of annual NAO and 32% for the winter, while the negative annual NAO occupies 16%,  
and 23% in the winter. However, the positive NAO condition does not persist throughout the entire years of droughts. Rather, it  
fluctuates from the positive to negative phases during multi-year droughts. Assessing the co-occurrence between droughts and  
cold Tropical Equatorial Pacific (La Niña-like) conditions, we find that during droughts, La Niña-like conditions are present  
415 in 37% of total drought periods, El Niño-like in 22%. Similar to NAO, La Niña-like conditions do not persist throughout the  
entire drought years.

The extreme positive NAO, defined as values above 95 percentiles of NAO during non-drought periods, occurs slightly more  
frequent during droughts, and the mean of this extreme NAO is statistically different from the mean extreme NAO during  
non-drought periods at 5% confidence level, for both annual and winter NAO (p-values from MW-U test of 0.02 for annual  
420 and 0.002 for winter). However, for ENSO, there is no statistically significant change in the mean and frequency of extreme La  
Niña-like condition compared to the non-drought periods.

To examine the behavior of the atmosphere during multi-years Mediterranean droughts, the frequency of modes of variability  
and mean composites of circulation during droughts are split in three stages: initiation, transition and termination years (Sect.  
2.3). The frequencies of occurrence of NAO and ENSO in each stage is presented in the Fig.9. The positive NAO occurs more  
425 frequently in the initiation years than in the transition and the termination years of droughts. The positive NAO occupies 49%  
in the initiation years, then it decreases throughout the development of droughts, falling to 29% in the termination years. The  
frequency of extreme positive NAO also decreases over time. In case of ENSO, the frequency of La Niña-like is 40% in the

initiation years. The occurrence of La Niña-like conditions increases slightly in the transition years, though, this increase is not statistically significant compared to the previous stage. Then, it decreases to 20% in the termination years. After the initiation  
430 years, there are increases in negative NAO and El Niño-like states. These changes in the frequencies of NAO and ENSO in each stage of droughts indicate a weakening role of large-scale circulation patterns at sustaining the persistence of droughts over time. As the intensities of droughts become more severe with their duration, some other factors need to be involved in sustaining the longevity of multi-years Mediterranean droughts from the transition to termination years.

The mean circulation and atmospheric conditions during the development of multi-years Mediterranean droughts are shown  
435 in the Fig. 10 depicted by the specific humidity, temperature, and winds at 925 hPa level. In the initiation years, the southerly winds prevail over the southern Mediterranean region. These southerlies block the intrusion of the westerly systems from the North Atlantic, and together with the cyclonic winds in the East Atlantic distribute dry and warm air masses from the East Atlantic, southern Mediterranean and west Africa to the continent. In the transition years, a complete anticyclonic circulation associated with the high over central Europe and the Mediterranean region is developed. This anticyclonic system distributes  
440 the dry and warm air to the north and west of the continent and sustains dry and warm condition over the region. During these years, the westerlies from the North Atlantic are clearly weakened. In the termination years, the anticyclonic circulation over Europe is not observed anymore, indicating a break-up of the high.

The mean circulation in each stage shows that the development of the high pressure system, namely the drought high in the Fig. 7, takes place in the transition years. This indicates that some mechanisms associated with this circulation is possibly  
445 important at determining the longevity of droughts after the initiation years. A possible candidate of an important process for the transition stage of Mediterranean droughts is the interaction among regional atmospheric and soil variables initiated by the anticyclonic circulation system over the region.

This is supported by the increases in frequencies of positive surface temperature (TS) and negative soil moisture (SOIL), evapotranspiration (EV), sensible (SH) and latent (LH) heat flux anomalies in the transition years (Fig.11). The mechanism  
450 associated with these regional atmospheric and soil variables is explained as follows: a decrease in precipitation supported by the positive NAO and/or La Niña-like induce initial regional dryness and a stable atmospheric condition associated with the increase in geopotential high anomaly (GP) over the region. A positive GP induces an initial increase in the regional TS. This positive TS decreases SOIL and EV. The latter increases SH and decreases LH during the initiation year. During the transition years, due to the stable atmospheric condition that still persists (positive GP) and the increase in SH and loss  
455 of LH in the previous stage, the positive TS is even magnified. TS in turn again increases SH, decreases EV and LH, thus, decreases SOIL. Over time, the complete high is developed and persists, fueling again this positive temperature - soil moisture feedback mechanism (Seneviratne et al., 2010; Yin et al., 2014). Thus, during the transient years, the means and occurrence of these variables associated with the feedback (positive TS, negative SOIL, negative EV, positive SH, negative LH) are clearly larger than their values during the initiation years (Fig.11). This mechanism continues until the termination years. During the  
460 termination years, the positive GP and TS still prevail over the region, though, with reduced anomalies. Also, the magnitudes of other variables are reduced compared to the previous stage.

This result indicates that once the drought high is developed, the temperature - soil moisture feedback is a more important mechanism than the connection to NAO and La Niña-like patterns in order to sustain the continuous depletion of soil moisture, which means the duration of droughts. Though the large scale circulation patterns help to support the regional dry conditions, after the initiation years, their roles in sustaining droughts are diminished.

### 3.5 Historical and Future condition on droughts: 1850 to 2099 AD

Here, the behavior of Mediterranean droughts as well as the associated mechanisms for the period 1850 - 2099 AD are presented. For an overview, the time series of the soil and precipitation anomalies (with respect to the mean of the period 1000 -1849 AD) over the Mediterranean region for the period 1850 - 2099 AD are shown in the Fig. 12. The simulation indicates that the region becomes drier for the period 1850 -2099 AD than the past, which is reflected in pronounced decreases in soil moisture and precipitation. The reduction in these two variables is already noticed from the beginning of 1850 AD concomitantly with the anthropogenic increase in GHG. By the end of the 21st century, the region experiences a constant drought situation without any wet anomaly with respect to the 1000 - 1849 AD condition. This indicates a shift of the mean climate of the region to a drier climate under the RCP 8.5 scenario, which is in line with other previous studies on the future projection of the region (e.g., Dubrovský et al., 2014; Naumann et al., 2018). Next, we analyze whether the mechanisms associated with Mediterranean droughts presented in the previous sections have changed during this period by comparing the non-detrended and detrended drought related variables. The detrending process is performed following the steps mentioned in the Sect. 2.2. In this way, we exclude the trends caused by the anthropogenic changes during these 250 years to observe the background climate during droughts.

Previously, it is shown that past Mediterranean droughts are associated with the intense positive geopotential height and temperature anomalies over central Europe and the Mediterranean. These features are also observed during droughts in the non-detrended 1850 - 2099 AD condition, but with more intense positive geopotential height (GP) and temperature (TS) anomalies than during the period 850 - 1849 AD (Fig. 13.(a)). The variances of GP, TS and SOIL are also enlarged compared to the past; therefore, their medians and extreme tails are also magnified, which imply that the dryness and its associated atmospheric conditions become more frequent and severe in 1850 - 2099 AD. The increases in GP and TS clearly intensify the above mentioned interaction among regional atmospheric and soil variables, i.e the positive temperature – soil moisture feedback. This intensification aids the longevity and intensity of droughts, which is also reflected as a reduction in the surface soil moisture anomaly (Fig. 9). Additionally, the precipitation - soil moisture interaction is involved, i.e. a continuous reduction in precipitation decreases soil moisture, thus, inducing less evapotranspiration, which leads again to a reduction in precipitation (Seneviratne et al., 2010).

Related to the modes of variability, the frequencies of positive NAO and La Niña-like conditions during droughts also seem to be affected by the overall change in global temperature (Fig. 13.(b)). Compared to 850 – 1849 AD, the non-detrended 1850 – 2099 AD period shows a slight reduction in the preference toward the positive NAO and La Niña-like conditions during droughts. This result is in line with the previously mentioned regional circulation associated with droughts: in this situation where the regional atmospheric variables have a more dominant role in the regional desiccation aided by the intense GP and

TS, the importance of modes of variability is reduced, even during the initial stages of droughts. Hence, the role of positive NAO and La Niña-like through different stages of droughts is diminished.

For the detrended variables, the means of GP and SOIL during droughts show that they are statistically indifferent to the 850-1849 AD values (p-value of 0.09 for GP and 0.44 for SOIL). The same is also true for the NAO and ENSO during droughts (p-values of 0.19 and 0.29 for each). The detrended TS over the region is statistically similar from the 850-1849 AD value but only at 2% confidence level (p-value of 0.02). This indicates that the detrending method is not enough to fully exclude the strong effects of anthropogenic changes on temperature in future droughts. Nevertheless, the mean spatial composites of the detrended surface temperature and geopotential height at 850 hPa during Mediterranean droughts (Fig. 14) support the indifference between these two periods over the large portion of the Mediterranean region, exhibiting the circulation patterns which are similar to those during the 850 - 1849 AD period (Fig. 7). This result shows that the natural mechanisms associated with droughts remain the same as it is in the past period, thus, no natural changes on drought mechanisms occur for the period of 1850 – 2099 AD. This means that the intensification of Mediterranean droughts is clearly due to the anthropogenic influences: in the future scenario, the intensity of atmosphere - soil feedback is magnified, due to the increase in GP and TS, and this mechanism becomes the dominant one at controlling the desiccation over the region.

#### 510 4 Conclusions

We have investigated the variability and mechanisms of multi-years droughts over the western and central Mediterranean region with pan-regional characteristic for the period of 850 - 1849 AD and whether these mechanisms associated with Mediterranean droughts have changed after the pre-industrial period from 1850 to 2099 AD with the anthropogenic increase in GHG. We have performed our analysis by using CESM simulations.

515 First of all, our result shows that though some overlapping years in drought periods among indices exist, the quantification of droughts is sensitive to the choice of drought index even in the paleoclimate context. For example, the scPDSI exhibits drought events with longer duration than the other indices, while the SPI is opposite, presenting more shorter lasting events. Though, the major mechanisms that induce multi-years droughts over the region remain similar due to the same overlapping periods and statistically significant correlation among indices, this discrepancy among indices can lead to a different conclusion, mostly in the number and duration of past drought events. This shows that using just one unique index is still complicated, even in the paleoclimate context. Hence, the uncertainty associated with different indices must be taken into account when comparing indices in drought studies (Dai, 2011; Raible et al., 2017; Mukherjee et al., 2018), in particular, in the case when only a single drought index is used and the focus is on the assessment of the duration of extreme hydrological events in past periods.

525 Secondly, we found that the past Mediterranean droughts are mainly induced by the internal dynamics of climate system supporting the finding of Xoplaki et al. (2018): the patterns of surface temperature and circulation over the Mediterranean during droughts in the control simulation is statistically indifferent from those of the transient simulation with full external forcing. A causal connection between volcanic eruptions and Mediterranean dry conditions was not identified, resembling findings of some previous studies, which indicate that past strong volcanic eruptions are more associated with wet events over

the region (McConnell et al., 2020; Rao et al., 2017). One of the distinct patterns found during Mediterranean droughts is a  
530 barotropic high pressure system accompanied by a positive temperature anomaly over central Europe and the Mediterranean  
region. This warm high persists during all seasons when droughts occur over the region, showing stronger intensity during  
winter and spring. This result emphasizes the importance of the wet cold seasons, i.e. winter and spring climate and circula-  
tion in annual Mediterranean droughts. Other patterns occurring during droughts are the positive NAO and the cold Tropical  
Equatorial Pacific (La Niña-like condition).

535 Thirdly, the mechanisms associated with sustaining multi-years droughts change through the stages of droughts. We found  
that these large-scale circulation patterns, such as the positive NAO and negative ENSO, play a more important role during  
the early stage of droughts, by providing dry condition over the western and central Mediterranean region to initiate such  
events. Then, the longevity of droughts is determined by the interaction of regional circulation variables, which involve stable  
atmospheric conditions, a temperature increase, changes in evapotranspiration and surface heat fluxes. Namely, this is the  
540 temperature - soil moisture feedback, which continues until the termination of droughts. During these transition years of  
droughts, the role played by the large-scale patterns is reduced. Hence, the persistence and duration of multi-years droughts  
should not be fully attributed to the states of large-scale circulation patterns, such as NAO and ENSO, as the roles of regional  
feedback and circulations on droughts become as important as or more important than large-scale modes after the initial  
development of droughts.

545 The model inherent biases in representing ENSO and NAO (Bellenger et al., 2014; Fasullo et al., 2020) can have some  
implications in our results on the frequencies of ENSO and NAO at different stages of droughts. The model may produce too  
frequent and strong La Niña conditions and positive NAO during droughts due to its amplified, decadal for ENSO and seasonal  
for NAO, variability. Moreover, due to the uncertainty associated with the changes in these modes in the future scenario,  
caution is required when interpreting the connection between droughts and modes of variability in the future warming scenario.  
550 Nonetheless, this problem does not affect our conclusion: the roles of ENSO and NAO become weaker with the longevity of  
droughts, while the regional circulation and feedback become more dominant at maintaining the persistence of droughts, which  
is also found in the future warming scenario.

555 Fourthly, the decreases in soil moisture and precipitation anomalies are already detected since the pre-industrial period  
concomitantly with the anthropogenic increase in GHG. This means that the intensification of droughts and the shift of the  
mean climate over the region to a drier climate have already started since the pre-industrial era. This regional desiccation is  
principally caused by the anthropogenic increase in GHG, which induces the intensification of interactions between the regional  
atmospheric and soil variables, associated with the temperature- soil moisture and precipitation - soil moisture feedbacks. If  
the increase in temperature and decreases in precipitation continue, intensifying the depletion of soil moisture in the future, the  
region will suffer from a continuous desiccation instead of droughts, as droughts are the deviation from the mean hydrological  
560 condition.

Fifthly, it is important to mention that our analysis is based on a single model output and this raises questions related to single  
model studies, such as boundary condition problems and model-dependent biases and physics (PAGES Hydro2k Consortium,  
2017). Nevertheless, for a small confined area that surrounds a large body of water mass, the Mediterranean Sea, and the land

coverage is limited, we found the necessity to use a simulation with a finer resolution to represent the regional climate better.  
565 In the end, our study provides a useful understanding on the long-term variability and mechanisms of Mediterranean droughts  
by analyzing the entire last millennium. We addressed the influences of external and internal variability on Mediterranean  
droughts and distinctly different roles of the large-scale modes of variability and regional circulation during the different stages  
of multi-year droughts.

Lastly, we emphasize again the importance of assessing different drought indices in the paleoclimate context, but also in  
570 the present and future warming scenario. Assessing different drought metrics is important for drought studies, as the most  
commonly used drought indices are based on water balance only from the atmospheric moisture supply and demand, and they  
tend to magnify drought risks in the future warming scenario (Berg et al., 2017; Mukherjee et al., 2018; Swann et al., 2016).  
For a more comprehensive picture, droughts need be quantified with indices that can also reflect water stress on plants and  
ecosystem, and complex interactions among soil, atmosphere and vegetation. We used the upper 10 cm soil moisture anomaly  
575 to partially tackle this issue and derived spatial patterns associated with Mediterranean droughts based on this index. Still, the  
upper 10 cm soil moisture does not fully involve a complex interaction in the soil and atmosphere occurring during droughts.  
As vegetation is known to have more complex responses to the changing climate and droughts (Swann, 2018; Swann et al.,  
2016), the role of vegetation in extreme hydrological events can provide a more comprehensive view on drought mechanisms.

The Mediterranean region is considered as one of the most vulnerable regions under the current climate change scenario  
580 (e.g. Giorgi and Lionello, 2008; Lehner et al., 2017) and human impacts can modify the natural mechanisms and propagation  
of droughts (Van Loon et al., 2016), increasing droughts risks and water shortage issues over the region. Hence, more studies  
on the topics related to droughts and permanent future desiccation in the Mediterranean region including the role of vegetation  
are necessary to develop a better preparedness for upcoming changes.

*Code availability.* Two R packages were used to calculate the drought indices: the *scPDSI* (Zhong et al., 2018) and the *SPEI* (Vicente-  
585 Serrano et al., 2009). The *biwavelet* (Gouhier et al., 2018) was used for the wavelength coherence analysis.

*Data availability.* The summer *scPDSI* from the Old World Drought Atlas (Cook et al., 2015) and the Sea Surface Temperature ERSST v5  
(Huang et al., 2017) are available on <https://www.ncdc.noaa.gov/>. The 20th Century Reanalysis V2 (Compo et al., 2011) and UDeI\_AirT\_Precip  
data (Willmott and Matsuura, 2001) are provided by the NOAA/OAR/ESRL PSL, Boulder, Colorado, USA, from their Web site at  
<https://psl.noaa.gov/>. The CESM simulations (Lehner et al., 2015) are available on request at the University of Bern.

590 *Author contributions.* WK and CR discussed and set up the initial research idea. WK performed the analysis and drafted the manuscript  
under the supervision of CR. CR provided critical feedback on the results and the manuscript. Both authors contributed to the interpretation  
and discussion of the results and edited the manuscript together.

*Competing interests.* The authors declare that they have no conflict of interest.

*Acknowledgements.* The study is funded by the Swiss National Science Foundation (SNSF, grant 200020\_172745). We acknowledge that  
595 some simulations were performed at the Swiss National Super Computing Centre (CSCS). Support for the Twentieth Century Reanalysis  
Project dataset is provided by the U.S. Department of Energy, Office of Science Innovative and Novel Computational Impact on Theory and  
Experiment (DOE INCITE) program, and Office of Biological and Environmental Research (BER), by the National Oceanic and Atmospheric  
Administration Climate Program Office, and by the National Oceanic and Atmospheric Administration Climate Program Office, and by the  
NOAA Physical Sciences Laboratory. The 20th Century Reanalysis V2 and UDel\_AirT\_Precip data are provided by the NOAA/OAR/ESRL  
600 PSL, Boulder, Colorado, USA, from their Web site at <https://psl.noaa.gov/>

## References

- Alpert, P., Neeman, B., and Shay-El, Y.: Climatological analysis of Mediterranean cyclones using ECMWF data, *Tellus A: Dynamic Meteorology and Oceanography*, 42, 65–77, <https://doi.org/10.3402/tellusa.v42i1.11860>, 1990.
- Babst, F., Bodesheim, P., Charney, N., Friend, A. D., Girardin, M. P., Klesse, S., Moore, D. J., Seftigen, K., Björklund, J., Bouriaud, O.,  
605 et al.: When tree rings go global: challenges and opportunities for retro-and prospective insight, *Quaternary Science Reviews*, 197, 1–20, <https://doi.org/10.1016/j.quascirev.2018.07.009>, 2018.
- Barnston, A. G. and Livezey, R. E.: Classification, seasonality and persistence of low-frequency atmospheric circulation patterns, *Monthly weather review*, 115, 1083–1126, [https://doi.org/10.1175/1520-0493\(1987\)115<1083:CSAPOL>2.0.CO;2](https://doi.org/10.1175/1520-0493(1987)115<1083:CSAPOL>2.0.CO;2), 1987.
- Bellenger, H., Guilyardi, É., Leloup, J., Lengaigne, M., and Vialard, J.: ENSO representation in climate models: From CMIP3 to CMIP5,  
610 *Climate Dynamics*, 42, 1999–2018, <https://doi.org/10.1007/s00382-013-1783-z>, 2014.
- Berg, A., Sheffield, J., and Milly, P. C.: Divergent surface and total soil moisture projections under global warming, *Geophysical Research Letters*, 44, 236–244, <https://doi.org/10.1002/2016GL071921>, 2017.
- Brönnimann, S.: Impact of El Niño–southern oscillation on European climate, *Reviews of Geophysics*, 45, <https://doi.org/10.1029/2006RG000199>, 2007.
- 615 Brönnimann, S., Xoplaki, E., Casty, C., Pauling, A., and Luterbacher, J.: ENSO influence on Europe during the last centuries, *Climate Dynamics*, 28, 181–197, <https://doi.org/10.1007/s00382-006-0175-z>, 2007.
- Champion, A. J., Hodges, K. I., Bengtsson, L. O., Keenlyside, N. S., and Esch, M.: Impact of increasing resolution and a warmer climate on extreme weather from Northern Hemisphere extratropical cyclones, *Tellus A: Dynamic meteorology and oceanography*, 63, 893–906, <https://doi.org/10.1111/j.1600-0870.2011.00538.x>, 2011.
- 620 Coats, S. and Karnauskas, K.: Are simulated and observed twentieth century tropical Pacific sea surface temperature trends significant relative to internal variability?, *Geophysical Research Letters*, 44, 9928–9937, <https://doi.org/10.1002/2017GL074622>, 2017.
- Coats, S., Smerdon, J. E., Seager, R., Cook, B. I., and González-Rouco, J. F.: Megadroughts in southwestern North America in ECHO-G millennial simulations and their comparison to proxy drought reconstructions, *Journal of climate*, 26, 7635–7649, <https://doi.org/10.1175/JCLI-D-12-00603.1>, 2013.
- 625 Coats, S., Smerdon, J. E., Cook, B., Seager, R., Cook, E. R., and Anchukaitis, K. J.: Internal ocean-atmosphere variability drives megadroughts in Western North America, *Geophysical research letters*, 43, 9886–9894, <https://doi.org/10.1002/2016GL070105>, 2016.
- Compo, G. P., Whitaker, J. S., Sardeshmukh, P. D., Matsui, N., Allan, R. J., Yin, X., Gleason, B. E., Vose, R. S., Rutledge, G., Bessemoulin, P., et al.: The twentieth century reanalysis project, *Quarterly Journal of the Royal Meteorological Society*, 137, 1–28, <https://doi.org/10.1002/qj.776>, 2011.
- 630 Cook, B. I., Anchukaitis, K. J., Touchan, R., Meko, D. M., and Cook, E. R.: Spatiotemporal drought variability in the Mediterranean over the last 900 years, *Journal of Geophysical Research: Atmospheres*, 121, 2060–2074, <https://doi.org/10.1002/2015JD023929>, 2016a.
- Cook, B. I., Cook, E. R., Smerdon, J. E., Seager, R., Williams, A. P., Coats, S., Stahle, D. W., and Díaz, J. V.: North American megadroughts in the Common Era: Reconstructions and simulations, *Wiley Interdisciplinary Reviews: Climate Change*, 7, 411–432, <https://doi.org/10.1002/wcc.394>, 2016b.
- 635 Cook, B. I., Mankin, J. S., and Anchukaitis, K. J.: Climate Change and Drought: From Past to Future, *Current Climate Change Reports*, 4, 164–179, <https://doi.org/10.1007/s40641-018-0093-2>, 2018.

- Cook, E. R., Seager, R., Kushnir, Y., Briffa, K. R., Büntgen, U., Frank, D., Krusic, P. J., Tegel, W., van der Schrier, G., Andreu-Hayles, L., et al.: Old World megadroughts and pluvials during the Common Era, *Science advances*, 1, e1500561, <https://doi.org/10.1126/sciadv.1500561>, 2015.
- 640 Dai, A.: Drought under global warming: a review, *Wiley Interdisciplinary Reviews: Climate Change*, 2, 45–65, <https://doi.org/10.1002/wcc.81>, 2011.
- Deser, C., Hurrell, J. W., and Phillips, A. S.: The role of the North Atlantic Oscillation in European climate projections, *Climate dynamics*, 49, 3141–3157, <https://doi.org/10.1007/s00382-016-3502-z>, 2017.
- Dubrovský, M., Hayes, M., Duce, P., Trnka, M., Svoboda, M., and Zara, P.: Multi-GCM projections of future drought and climate variability indicators for the Mediterranean region, *Regional Environmental Change*, 14, 1907–1919, <https://doi.org/10.1007/s10113-013-0562-z>, 2014.
- 645 Dünkeloh, A. and Jacobeit, J.: Circulation dynamics of Mediterranean precipitation variability 1948–98, *International Journal of Climatology: A Journal of the Royal Meteorological Society*, 23, 1843–1866, <https://doi.org/10.1002/joc.973>, 2003.
- Fasullo, J. T., Phillips, A., and Deser, C.: Evaluation of Leading Modes of Climate Variability in the CMIP Archives, *Journal of Climate*, 33, 5527–5545, <https://doi.org/10.1175/JCLI-D-19-1024.1>, 2020.
- 650 Field, C. B., Barros, V., Stocker, T. F., and Dahe, Q.: Managing the risks of extreme events and disasters to advance climate change adaptation: special report of the intergovernmental panel on climate change, Cambridge University Press, 2012.
- Franke, J., Frank, D., Raible, C. C., Esper, J., and Brönnimann, S.: Spectral biases in tree-ring climate proxies, *Nature Climate Change*, 3, 360–364, <https://doi.org/10.1038/nclimate1816>, 2013.
- 655 Gao, C., Robock, A., and Ammann, C.: Volcanic forcing of climate over the past 1500 years: An improved ice core-based index for climate models, *Journal of Geophysical Research: Atmospheres*, 113, <https://doi.org/10.1029/2008JD010239>, 2008.
- García-Herrera, R., Garrido-Perez, J. M., Barriopedro, D., Ordóñez, C., Vicente-Serrano, S. M., Nieto, R., Gimeno, L., Sorí, R., and Yiou, P.: The European 2016/17 Drought, *Journal of Climate*, 32, 3169–3187, <https://doi.org/10.1175/JCLI-D-18-0331.1>, 2019.
- Giorgi, F.: Climate change hot-spots, *Geophysical research letters*, 33, <https://doi.org/10.1029/2006GL025734>, 2006.
- 660 Giorgi, F. and Lionello, P.: Climate change projections for the Mediterranean region, *Global and Planetary Change*, 63, 90–104, <https://doi.org/10.1016/j.gloplacha.2007.09.005>, 2008.
- Gouhier, T. C., Grinsted, A., and Simko, V.: R package biwavelet: Conduct Univariate and Bivariate Wavelet Analyses, <https://github.com/tgouhier/biwavelet>, (Version 0.20.17), 2018.
- Grinsted, A., Moore, J. C., and Jevrejeva, S.: Application of the cross wavelet transform and wavelet coherence to geophysical time series, *Nonlinear Processes in Geophysics*, 11, 561–566, <https://hal.archives-ouvertes.fr/hal-00302394>, publisher: European Geosciences Union (EGU), 2004.
- 665 Haywood, A. M., Valdes, P. J., Aze, T., Barlow, N., Burke, A., Dolan, A. M., von der Heydt, A. S., Hill, D. J., Jamieson, S. S. R., Otto-Bliesner, B. L., Salzmann, U., Saupe, E., and Voss, J.: What can Palaeoclimate Modelling do for you?, *Earth Systems and Environment*, 3, 1–18, <https://doi.org/10.1007/s41748-019-00093-1>, 2019.
- 670 Hoerling, M., Eischeid, J., Perlwitz, J., Quan, X., Zhang, T., and Pegion, P.: On the Increased Frequency of Mediterranean Drought, *Journal of Climate*, 25, 2146–2161, <https://doi.org/10.1175/JCLI-D-11-00296.1>, 2011.
- Huang, B., Thorne, P. W., Banzon, V. F., Boyer, T., Chepurin, G., Lawrimore, J. H., Menne, M. J., Smith, T. M., Vose, R. S., and Zhang, H.-M.: Extended reconstructed sea surface temperature, version 5 (ERSSTv5): upgrades, validations, and intercomparisons, *Journal of Climate*, 30, 8179–8205, <https://doi.org/10.1175/JCLI-D-16-0836.1>, 2017.

- 675 Hurrell, J. W.: Decadal trends in the North Atlantic Oscillation: regional temperatures and precipitation, *Science*, 269, 676–679, <https://doi.org/10.1126/science.269.5224.676>, 1995.
- Krichak, S. O. and Alpert, P.: Decadal trends in the east Atlantic–west Russia pattern and Mediterranean precipitation, *International journal of climatology: a journal of the Royal Meteorological Society*, 25, 183–192, <https://doi.org/10.1002/joc.1124>, 2005.
- Lehner, F., Joos, F., Raible, C. C., Mignot, J., Born, A., Keller, K. M., and Stocker, T. F.: Climate and carbon cycle dynamics in a CESM  
680 simulation from 850 to 2100 CE, *Earth System Dynamics*, 6, 411–434, <https://doi.org/10.5194/esd-6-411-2015>, 2015.
- Lehner, F., Coats, S., Stocker, T. F., Pendergrass, A. G., Sanderson, B. M., Raible, C. C., and Smerdon, J. E.: Projected drought risk in 1.5°C and 2°C warmer climates, *Geophysical Research Letters*, 44, 7419–7428, <https://doi.org/10.1002/2017GL074117>, 2017.
- Li, W., Li, L., Ting, M., and Liu, Y.: Intensification of Northern Hemisphere subtropical highs in a warming climate, *Nature Geoscience*, 5, 830–834, <https://doi.org/10.1038/ngeo1590>, 2012.
- 685 Lionello, P., Malanotte-Rizzoli, P., Boscolo, R., Alpert, P., Artale, V., Li, L., Luterbacher, J., May, W., Trigo, R., Tsimplis, M., Ulbrich, U., and Xoplaki, E.: The Mediterranean climate: An overview of the main characteristics and issues, in: *Developments in Earth and Environmental Sciences*, edited by Lionello, P., Malanotte-Rizzoli, P., and Boscolo, R., vol. 4 of *Mediterranean*, pp. 1–26, Elsevier, [https://doi.org/10.1016/S1571-9197\(06\)80003-0](https://doi.org/10.1016/S1571-9197(06)80003-0), 2006.
- Lionello, P., Trigo, I. F., Gil, V., Liberato, M. L., Nissen, K. M., Pinto, J. G., Raible, C. C., Reale, M., Tanzarella, A., Trigo, R. M., et al.:  
690 Objective climatology of cyclones in the Mediterranean region: a consensus view among methods with different system identification and tracking criteria, *Tellus A: Dynamic Meteorology and Oceanography*, 68, 29391, <https://doi.org/10.3402/tellusa.v68.29391>, 2016.
- Liu, W., Sun, F., Lim, W. H., Zhang, J., Wang, H., Shiogama, H., and Zhang, Y.: Global drought and severe drought-affected populations in 1.5 and 2 C warmer worlds, *Earth System Dynamics*, 9, 267, <https://doi.org/10.5194/esd-9-267-2018>, 2018.
- Ljungqvist, F. C., Seim, A., Krusic, P. J., González-Rouco, J. F., Werner, J. P., Cook, E. R., Zorita, E., Luterbacher, J., Xoplaki, E.,  
695 Destouni, G., García-Bustamante, E., Aguilar, C. A. M., Seftigen, K., Wang, J., Gagen, M. H., Esper, J., Solomina, O., Fleitmann, D., and Büntgen, U.: European warm-season temperature and hydroclimate since 850 CE, *Environmental Research Letters*, 14, 084015, <https://doi.org/10.1088/1748-9326/ab2c7e>, 2019.
- Lloyd-Hughes, B.: The impracticality of a universal drought definition, *Theoretical and Applied Climatology*, 117, 607–611, <https://doi.org/10.1007/s00704-013-1025-7>, 2014.
- 700 Mariotti, A., Zeng, N., and Lau, K.-M.: Euro-Mediterranean rainfall and ENSO—a seasonally varying relationship, *Geophysical research letters*, 29, 59–1, <https://doi.org/10.1029/2001GL014248>, 2002.
- Mariotti, A., Zeng, N., Yoon, J.-H., Artale, V., Navarra, A., Alpert, P., and Li, L. Z.: Mediterranean water cycle changes: transition to drier 21st century conditions in observations and CMIP3 simulations, *Environmental Research Letters*, 3, 044001, <https://doi.org/10.1088/1748-9326/3/4/044001>, 2008.
- 705 McConnell, J. R., Sigl, M., Plunkett, G., Burke, A., Kim, W. M., Raible, C. C., Wilson, A. I., Manning, J. G., Ludlow, F., Chellman, N. J., et al.: Extreme climate after massive eruption of Alaska’s Okmok volcano in 43 BCE and effects on the late Roman Republic and Ptolemaic Kingdom, *Proceedings of the National Academy of Sciences*, 117, 15443–15449, <https://doi.org/10.1073/pnas.2002722117>, 2020.
- McKee, T. B., Doesken, N. J., Kleist, J., et al.: The relationship of drought frequency and duration to time scales, in: *Proceedings of the 8th Conference on Applied Climatology*, vol. 17, pp. 179–183, American Meteorological Society Boston, MA, 1993.
- 710 Mishra, A. K. and Singh, V. P.: A review of drought concepts, *Journal of hydrology*, 391, 202–216, <https://doi.org/10.1016/j.jhydrol.2010.07.012>, 2010.

- Mukherjee, S., Mishra, A., and Trenberth, K. E.: Climate Change and Drought: a Perspective on Drought Indices, *Current Climate Change Reports*, 4, 145–163, <https://doi.org/10.1007/s40641-018-0098-x>, 2018.
- 715 Namias, J.: Factors in the initiation, perpetuation and termination of drought, *International Association of Scientific Hydrology Commission on Surface Waters Publication*, 51, 81–94, 1960.
- Naumann, G., Alfieri, L., Wyser, K., Mentaschi, L., Betts, R., Carrao, H., Spinoni, J., Vogt, J., and Feyen, L.: Global changes in drought conditions under different levels of warming, *Geophysical Research Letters*, 45, 3285–3296, <https://doi.org/10.1002/2017GL076521>, 2018.
- Otto-Bliesner, B. L., Brady, E. C., Fasullo, J., Jahn, A., Landrum, L., Stevenson, S., Rosenbloom, N., Mai, A., and Strand, G.: Climate 720 variability and change since 850 CE: An ensemble approach with the Community Earth System Model, *Bulletin of the American Meteorological Society*, 97, 735–754, <https://doi.org/10.1175/BAMS-D-14-00233.1>, 2016.
- PAGES Hydro2k Consortium: Comparing proxy and model estimates of hydroclimate variability and change over the Common Era. *Clim Past* 13: 1851–1900, <https://doi.org/10.5194/cp-13-1851-2017>, 2017.
- Palmer, W. C.: *Meteorological drought*, vol. 30, US Department of Commerce, Weather Bureau, 1965.
- 725 Parsons, L. A. and Coats, S.: Ocean-atmosphere trajectories of extended drought in Southwestern North America, *Journal of Geophysical Research: Atmospheres*, 124, 8953–8971, <https://doi.org/10.1029/2019JD030424>, 2019.
- Parsons, L. A., Loope, G. R., Overpeck, J. T., Ault, T. R., Stouffer, R., and Cole, J. E.: Temperature and precipitation variance in CMIP5 simulations and paleoclimate records of the last millennium, *Journal of Climate*, 30, 8885–8912, <https://doi.org/10.1175/JCLI-D-16-0863.1>, 2017.
- 730 Parsons, L. A., Coats, S., and Overpeck, J. T.: The continuum of drought in Southwestern North America, *Journal of Climate*, 31, 8627–8643, <https://doi.org/10.1175/JCLI-D-18-0010.1>, 2018.
- Philandras, C., Nastos, P., Kapsomenakis, J., Douvis, K., Tselioudis, G., and Zerefos, C.: Long term precipitation trends and variability within the Mediterranean region, *Natural Hazards and Earth System Sciences*, 11, 3235, <https://doi.org/10.5194/nhess-11-3235-2011>, 2011.
- Previdi, M. and Liepert, B. G.: Annular modes and Hadley cell expansion under global warming, *Geophysical Research Letters*, 34, 735 <https://doi.org/10.1029/2007GL031243>, 2007.
- Raible, C.: On the relation between extremes of midlatitude cyclones and the atmospheric circulation using ERA40, *Geophysical research letters*, 34, <https://doi.org/10.1029/2006GL029084>, 2007.
- Raible, C., Luksch, U., Fraedrich, K., and Voss, R.: North Atlantic decadal regimes in a coupled GCM simulation, *Climate Dynamics*, 18, 321–330, 2001.
- 740 Raible, C., Yoshimori, M., Stocker, T., and Casty, C.: Extreme midlatitude cyclones and their implications for precipitation and wind speed extremes in simulations of the Maunder Minimum versus present day conditions, *Climate Dynamics*, 28, 409–423, <https://doi.org/10.1007/s00382-006-0188-7>, 2007.
- Raible, C. C., Luksch, U., and Fraedrich, K.: Precipitation and northern hemisphere regimes, *Atmospheric Science Letters*, 5, 43–55, <https://doi.org/10.1016/j.atmoscilet.2003.12.001>, 2003.
- 745 Raible, C. C., Ziv, B., Saaroni, H., and Wild, M.: Winter synoptic-scale variability over the Mediterranean Basin under future climate conditions as simulated by the ECHAM5, *Climate dynamics*, 35, 473–488, <https://doi.org/10.1007/s00382-009-0678-5>, 2010.
- Raible, C. C., Bärenbold, O., and Gómez-navarro, J. J.: Drought indices revisited – improving and testing of drought indices in a simulation of the last two millennia for Europe, *Tellus A: Dynamic Meteorology and Oceanography*, 69, 1287–492, <https://doi.org/10.1080/16000870.2017.1296226>, 2017.

- 750 Rao, M. P., Cook, B. I., Cook, E. R., D'Arrigo, R. D., Krusic, P. J., Anchukaitis, K. J., LeGrande, A. N., Buckley, B. M., Davi, N. K., Leland, C., and Griffin, K. L.: European and Mediterranean hydroclimate responses to tropical volcanic forcing over the last millennium, *Geophysical Research Letters*, 44, 5104–5112, <https://doi.org/10.1002/2017GL073057>, 2017.
- Schmidt, G. A., Jungclaus, J. H., Ammann, C. M., Bard, E., Braconnot, P., Crowley, T. J., Delaygue, G., Joos, F., Krivova, N. A., Muscheler, R., Otto-Bliesner, B. L., Pongratz, J., Shindell, D. T., Solanki, S. K., Steinhilber, F., and Vieira, L. E. A.: Climate forcing reconstructions  
755 for use in PMIP simulations of the Last Millennium (v1.1), *Geoscientific Model Development*, pp. 185–191, <https://doi.org/10.5194/gmd-5-185-2012>, 2012.
- Seager, R., Liu, H., Henderson, N., Simpson, I., Kelley, C., Shaw, T., Kushnir, Y., and Ting, M.: Causes of Increasing Aridification of the Mediterranean Region in Response to Rising Greenhouse Gases, *Journal of Climate*, 27, 4655–4676, <https://doi.org/10.1175/JCLI-D-13-00446.1>, 2014.
- 760 Seneviratne, S. I., Corti, T., Davin, E. L., Hirschi, M., Jaeger, E. B., Lehner, I., Orlowsky, B., and Teuling, A. J.: Investigating soil moisture–climate interactions in a changing climate: A review, *Earth-Science Reviews*, 99, 125–161, <https://doi.org/10.1016/j.earscirev.2010.02.004>, 2010.
- Sousa, P. M., Trigo, R. M., Aizpurua, P., Nieto, R., Gimeno, L., and Garcia-Herrera, R.: Trends and extremes of drought indices throughout the 20th century in the Mediterranean, *Natural Hazards and Earth System Sciences*, 11, 33–51, <https://doi.org/10.5194/nhess-11-33-2011>,  
765 2011.
- Spinoni, J., Naumann, G., Vogt, J. V., and Barbosa, P.: The biggest drought events in Europe from 1950 to 2012, *Journal of Hydrology: Regional Studies*, 3, 509–524, <https://doi.org/10.1016/j.ejrh.2015.01.001>, 2015.
- Spinoni, J., Naumann, G., and Vogt, J. V.: Pan-European seasonal trends and recent changes of drought frequency and severity, *Global and Planetary Change*, 148, 113–130, <https://doi.org/10.1016/j.gloplacha.2016.11.013>, 2017.
- 770 Stevenson, S., Overpeck, J. T., Fasullo, J., Coats, S., Parsons, L., Otto-Bliesner, B., Ault, T., Loope, G., and Cole, J.: Climate variability, volcanic forcing, and last millennium hydroclimate extremes, *Journal of Climate*, 31, 4309–4327, <https://doi.org/10.1175/JCLI-D-17-0407.1>, 2018.
- Swann, A. L.: Plants and drought in a changing climate, *Current Climate Change Reports*, 4, 192–201, <https://doi.org/10.1007/s40641-018-0097-y>, 2018.
- 775 Swann, A. L., Hoffman, F. M., Koven, C. D., and Randerson, J. T.: Plant responses to increasing CO<sub>2</sub> reduce estimates of climate impacts on drought severity, *Proceedings of the National Academy of Sciences*, 113, 10019–10024, <https://doi.org/10.1073/pnas.1604581113>, 2016.
- Thornthwaite, C. W. et al.: An approach toward a rational classification of climate, *Geographical review*, 38, 55–94, <https://doi.org/10.2307/210739>, 1948.
- Trenberth, K. E.: The Definition of El Niño, *Bulletin of the American Meteorological Society*, 78, 2771–2778, [https://doi.org/10.1175/1520-0477\(1997\)078<2771:TDOENO>2.0.CO;2](https://doi.org/10.1175/1520-0477(1997)078<2771:TDOENO>2.0.CO;2), 1997.  
780
- Trigo, R., Osborn, T., and Corte-Real, J.: The North Atlantic Oscillation influence on Europe: climate impacts and associated physical mechanisms, *Climate Research*, 20, 9–17, <https://doi.org/10.3354/cr020009>, 2002.
- Ulbrich, U., Leckebusch, G., and Pinto, J. G.: Extra-tropical cyclones in the present and future climate: a review, *Theoretical and Applied Climatology*, 96, 117–131, <https://doi.org/10.1007/s00704-008-0083-8>, 2009.
- 785 Van Loon, A. F., Gleeson, T., Clark, J., Van Dijk, A. I., Stahl, K., Hannaford, J., Di Baldassarre, G., Teuling, A. J., Tallaksen, L. M., Uijlenhoet, R., et al.: Drought in the Anthropocene, *Nature Geoscience*, 9, 89, <https://doi.org/10.1038/ngeo2646>, 2016.

- Vicente-Serrano, S. M.: El Niño and La Niña influence on droughts at different timescales in the Iberian Peninsula, *Water Resources Research*, 41, <https://doi.org/10.1029/2004WR003908>, 2005.
- Vicente-Serrano, S. M., Beguería, S., and López-Moreno, J. I.: A Multiscalar Drought Index Sensitive to Global Warming: The Standardized Precipitation Evapotranspiration Index, *Journal of Climate*, 23, 1696–1718, <https://doi.org/10.1175/2009JCLI2909.1>, 2009.
- Vicente-Serrano, S. M., Beguería, S., López-Moreno, J. I., Angulo, M., and El Kenawy, A.: A new global 0.5 gridded dataset (1901–2006) of a multiscalar drought index: comparison with current drought index datasets based on the Palmer Drought Severity Index, *Journal of Hydrometeorology*, 11, 1033–1043, <https://doi.org/10.1175/2010JHM1224.1>, 2010.
- Vicente-Serrano, S. M., Lopez-Moreno, J.-I., Beguería, S., Lorenzo-Lacruz, J., Arturo Sanchez-Lorenzo, García-Ruiz, J. M., Azorin-Molina, C., Morán-Tejeda, E., Revuelto, J., Ricardo Trigo, Coelho, F., and Espejo, F.: Evidence of increasing drought severity caused by temperature rise in southern Europe, *Environmental Research Letters*, 9, 044001, <https://doi.org/10.1088/1748-9326/9/4/044001>, 2014.
- Vicente-Serrano, S. M., Van der Schrier, G., Beguería, S., Azorin-Molina, C., and Lopez-Moreno, J.-I.: Contribution of precipitation and reference evapotranspiration to drought indices under different climates, *Journal of Hydrology*, 526, 42–54, <https://doi.org/10.1016/j.jhydrol.2014.11.025>, 2015.
- Wallace, J. M. and Gutzler, D. S.: Teleconnections in the Geopotential Height Field during the Northern Hemisphere Winter, *Monthly Weather Review*, 109, 784–812, [https://doi.org/10.1175/1520-0493\(1981\)109<0784:TITGHF>2.0.CO;2](https://doi.org/10.1175/1520-0493(1981)109<0784:TITGHF>2.0.CO;2), 1981.
- Wang, W., Ertsen, M. W., Svoboda, M. D., and Hafeez, M.: Propagation of drought: from meteorological drought to agricultural and hydrological drought, <https://doi.org/10.1155/2016/6547209>, 2016.
- Watterson, I.: The intensity of precipitation during extratropical cyclones in global warming simulations: a link to cyclone intensity?, *Tellus A: Dynamic Meteorology and Oceanography*, 58, 82–97, <https://doi.org/j.1600-0870.2006.00147.x>, 2006.
- Wells, N., Goddard, S., and Hayes, M. J.: A Self-Calibrating Palmer Drought Severity Index, *Journal of Climate*, 17, 2335–2351, [https://doi.org/10.1175/1520-0442\(2004\)017<2335:ASPDSE>2.0.CO;2](https://doi.org/10.1175/1520-0442(2004)017<2335:ASPDSE>2.0.CO;2), 2004.
- Wilhite, D.: Understanding the Phenomenon of Drought, Drought Mitigation Center Faculty Publications, <https://digitalcommons.unl.edu/droughtfacpub/50>, 1993.
- Willmott, C. J. and Matsuura, K.: Terrestrial air temperature and precipitation: Monthly and annual time series (1950–1999) Version 1.02, Center for Climatic Research, University of Delaware, Newark, 2001.
- Xoplaki, E., González-Rouco, J. F., Luterbacher, J., and Wanner, H.: Mediterranean summer air temperature variability and its connection to the large-scale atmospheric circulation and SSTs, *Climate Dynamics*, 20, 723–739, <https://doi.org/10.1007/s00382-003-0304-x>, 2003.
- Xoplaki, E., González-Rouco, J., Luterbacher, J., and Wanner, H.: Wet season Mediterranean precipitation variability: influence of large-scale dynamics and trends, *Climate dynamics*, 23, 63–78, 2004.
- Xoplaki, E., Luterbacher, J., Wagner, S., Zorita, E., Fleitmann, D., Preiser-Kapeller, J., Sargent, A. M., White, S., Toreti, A., Haldon, J. F., Mordechai, L., Bozkurt, D., Akçer-Ön, S., and Izdebski, A.: Modelling Climate and Societal Resilience in the Eastern Mediterranean in the Last Millennium, *Human Ecology*, 46, 363–379, <https://doi.org/10.1007/s10745-018-9995-9>, 2018.
- Yin, D., Roderick, M. L., Leech, G., Sun, F., and Huang, Y.: The contribution of reduction in evaporative cooling to higher surface air temperatures during drought, *Geophysical Research Letters*, 41, 7891–7897, <https://doi.org/10.1002/2014GL062039>, 2014.
- Zhong, R., Chen, X., Wang, Z., and Lai, C.: scPDSI: Calculation of the Conventional and Self-Calibrating Palmer Drought Severity Index, <https://CRAN.R-project.org/package=scPDSI>, r package version 0.1.3, 2018.
- Zhu, Y., Liu, Y., Wang, W., Singh, V. P., Ma, X., and Yu, Z.: Three dimensional characterization of meteorological and hydrological droughts and their probabilistic links, *Journal of Hydrology*, 578, 124016, <https://doi.org/10.1016/j.jhydrol.2019.124016>, 2019.

825 Zveryaev, I. I.: Seasonality in precipitation variability over Europe, *Journal of Geophysical Research: Atmospheres*, 109, <https://doi.org/10.1029/2003JD003668>, 2004.

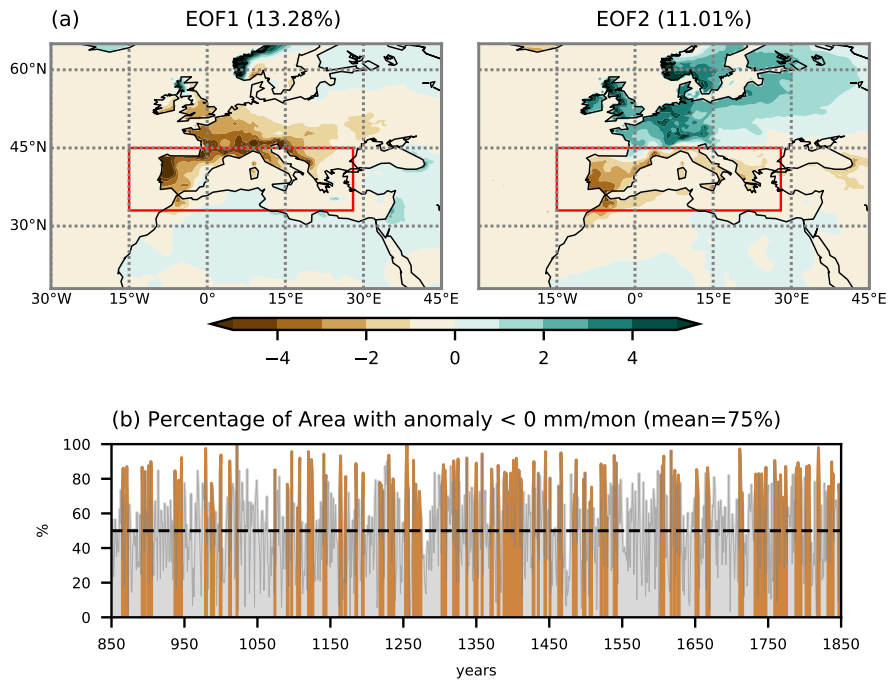


**Figure 1.** (a) Variance explained by the first EOF and second EOF in the observed monthly precipitation from U.Delaware v5.01 dataset for the period of 1901 – 2000 AD. The red rectangle indicates our region of study: west- and central Mediterranean. (b) Percentage of area with the soil moisture anomaly below  $0 \text{ mm}\cdot\text{mon}^{-1}$  in the region of study during the last millennium in CESM. Shaded in brown indicates years with droughts.

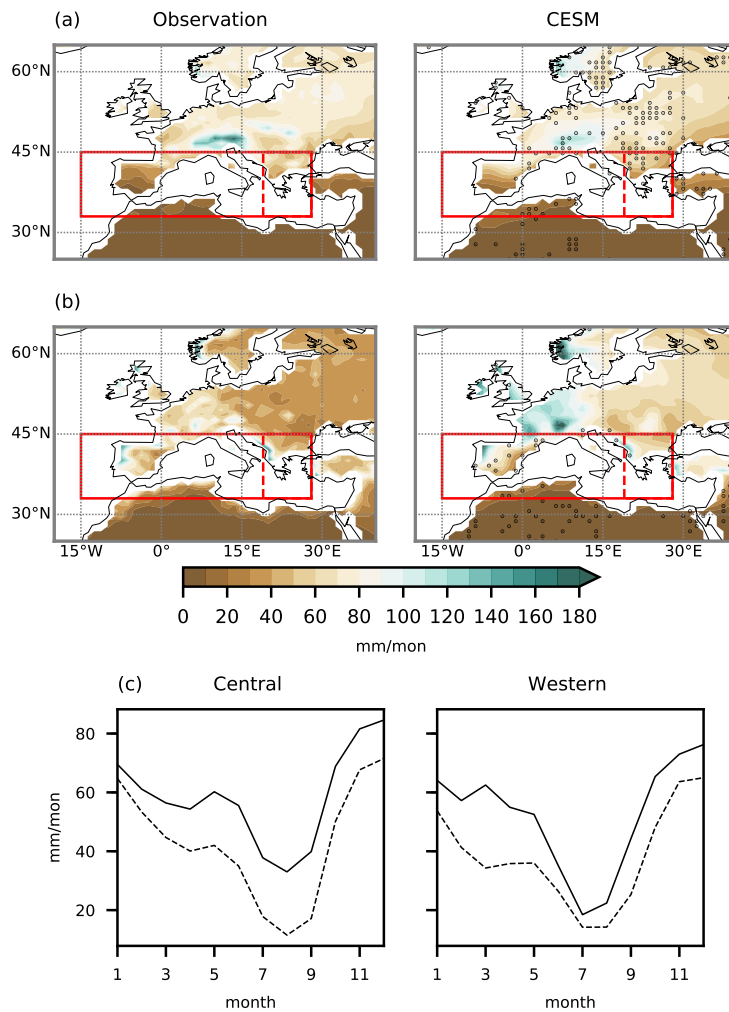


**Figure 2.** Mean seasonal precipitation for the observation (left) and CESM (right) in the (a) summer and (b) winter for the period of 1901 – 2000 AD. Black dots on the composites of CESM indicate the regions where the means between the observation and model are not statistically similar at 5% confidence level. (c) Mean annual cycles of precipitation for the same period over the areas in the rectangles. The observation is in continuous lines and CESM in dashed lines.

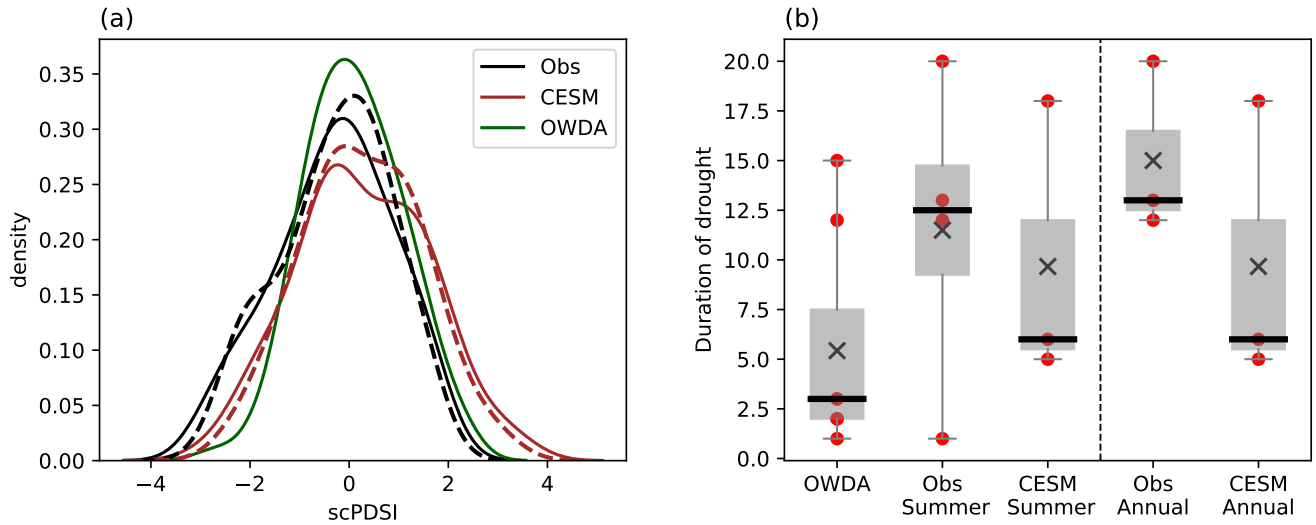


**Figure 3.** (a) Probabilistic distribution of monthly self-calibrated Palmer Drought Severity Indices (scPDSI) from the observation (black), CESM (red) and OWDA (green) smoothed by kernel density estimate using Gaussian kernels. Continuous lines indicate the summer and dashed lines the annual scPDSIs. The p-value from the t-student test between the summer scPDSI from CESM and OWDA is 0.28. The p-value between the OWDA and observation is 0.01, and between the CESM and Observation for the summer and annual, both p-values are 0.001. (b) Distribution of duration of annual-scale droughts in different datasets. Red points on each box shows the data points, thus number of droughts, black lines are the medians and crosses are the mean values of duration.

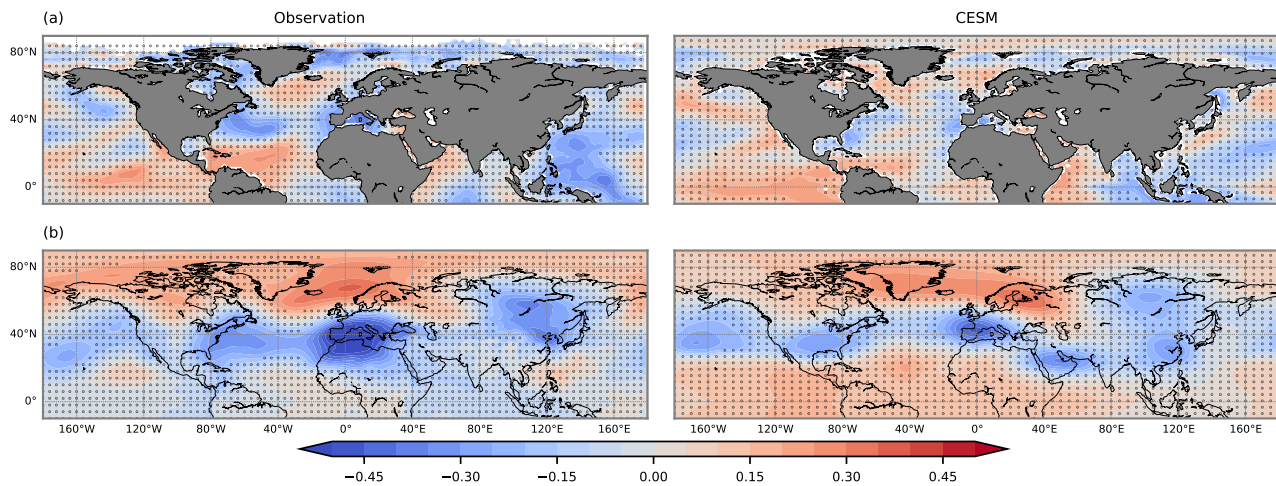


**Figure 4.** Maps of Pearson correlation between the scPDSI and anomalies of (a) Sea Surface Temperature from ERSST v5 and (b) Geopotential height at 850 hPa from the CR21 for the observation (left) and CESM (right) during the period of 1901-2000 AD. The linear trends of variables are removed before applying the correlation. Black dots on the maps show the regions where correlations are statistically not significant at 5% confidence level.

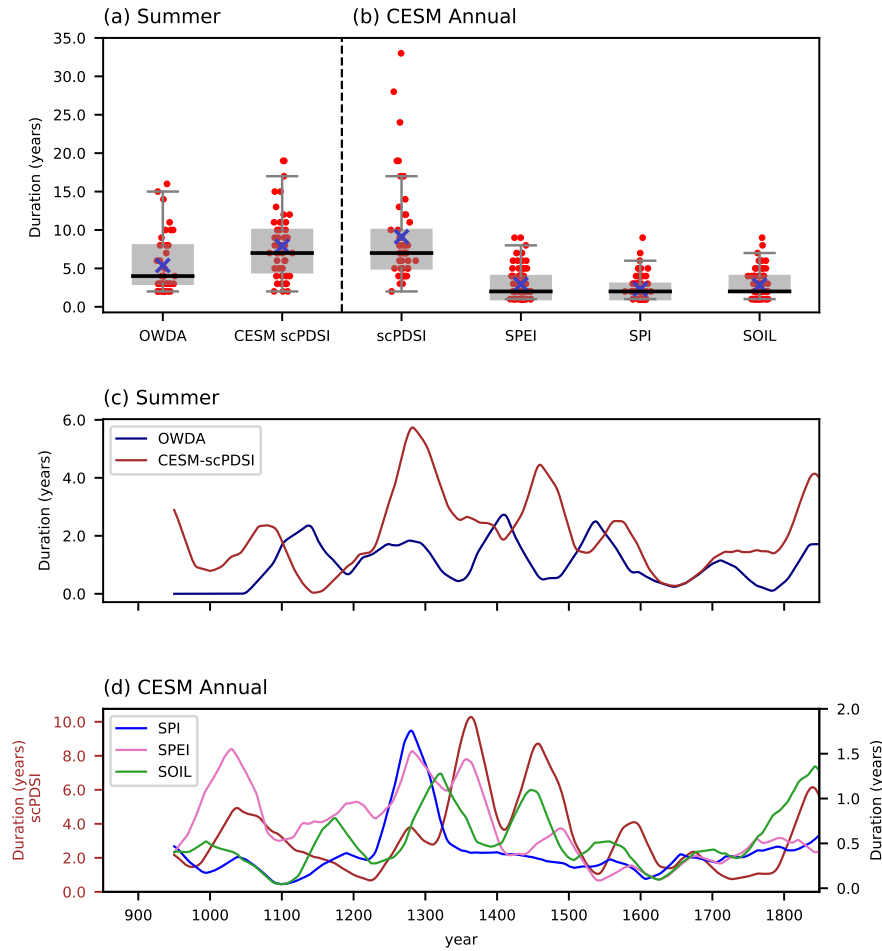


**Figure 5.** (a) Distribution of duration of droughts for the summer scPDSIs in OWDA and CESM, and for (b) the annual drought indices in CESM during 850 – 1849 AD. Red points indicate individual drought events, black lines on the boxes are the medians and blue crosses are the means of duration. (c) 100-years running means of duration of droughts for the summer scPDSIs and (d) the annual drought indices. The indices are the scPDSI from Old World Drought Atlas (OWDA), summer scPDSI from CESM (CESM-scPDSI), annual Standardized Precipitation Index (SPI), Standardized Precipitation Evapotranspiration Index (SPEI), soil moisture anomaly (SOIL), and annual scPDSI. Note that the annual scPDSI (brown line in (d)) has a separate y-axis for its duration. The p-value from Mann-Whitney U-test between the duration of summer scPDSI in OWDA and CESM is 0.003, which indicates the means are statistically different. For the annual indices, the means are also statistically different among each other, except between the SPEI and SOIL (p-value of 0.87).

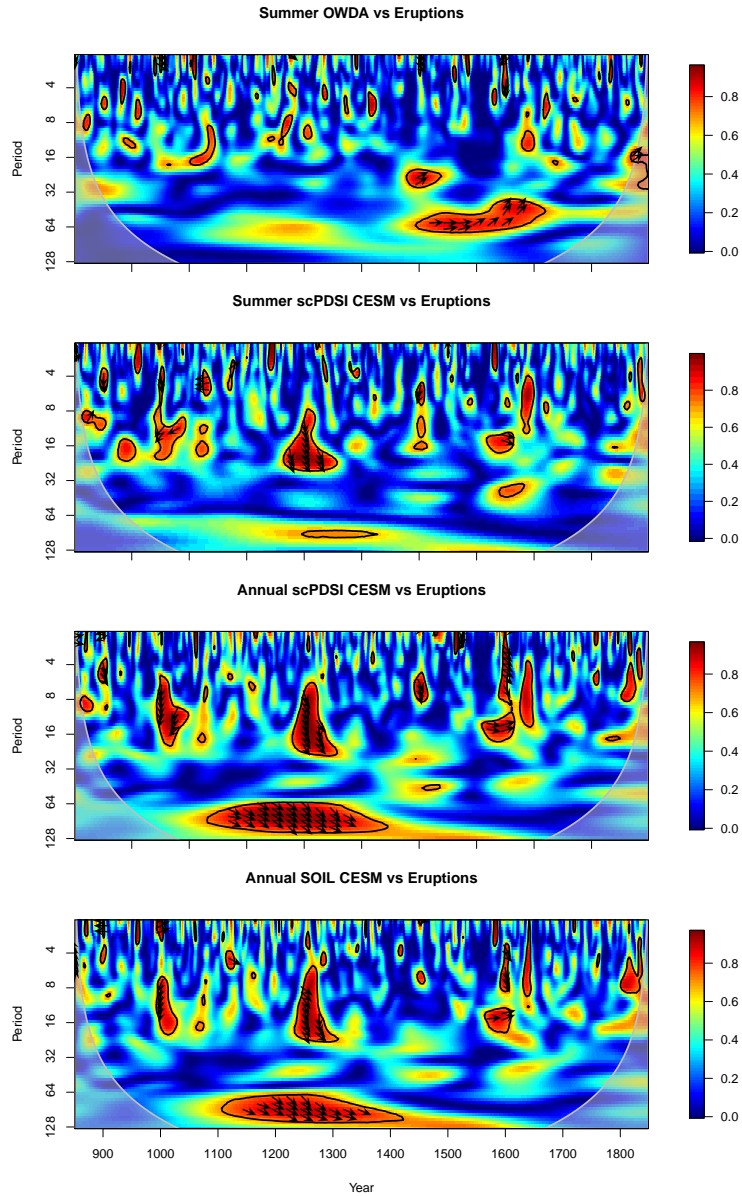


**Figure 6.** Wavelength coherence between drought indices (OWDA, summer and annual CESM scPDSI, and SOIL) and volcanic eruptions for 850 – 1849 AD. The red shaded regions indicate where the coherence of two time series are statistically significant at 5% confidence level. The directions of arrow provide information on the association between two variables, whether they are in-phase (to the right) or anti-phase (to the left), the first variable (right-down or left-up) or the second variable (right-up or left-down) plays the causal role.

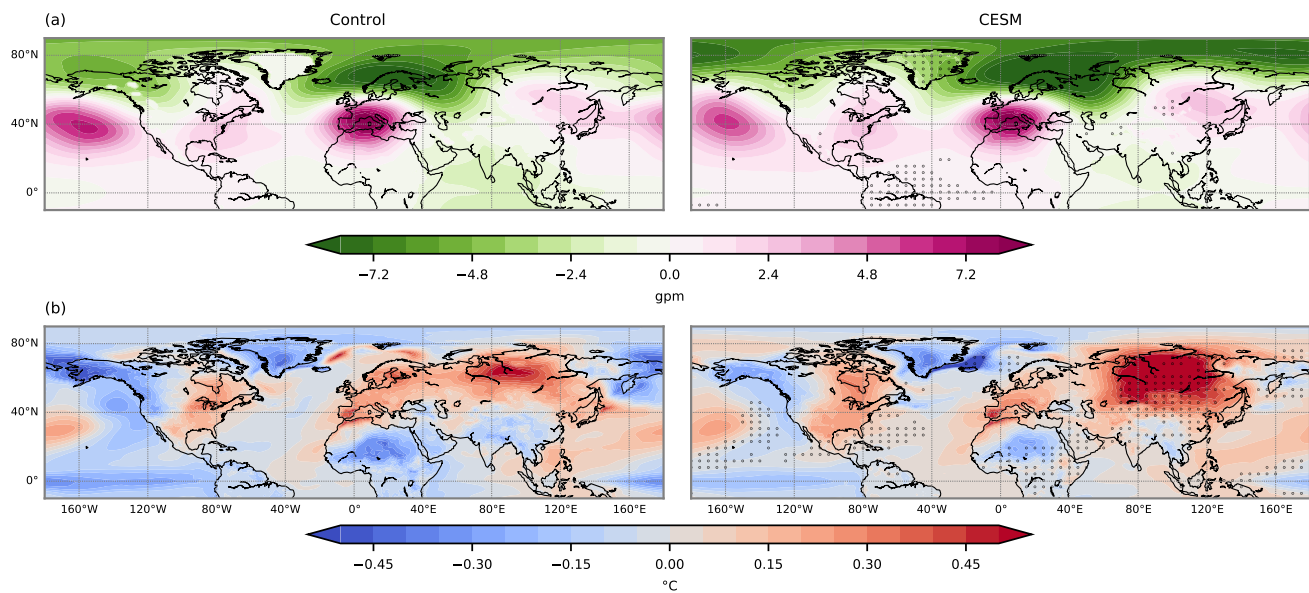


**Figure 7.** (a) Mean geopotential height anomaly at 850 hpa, and (b) mean surface temperature anomaly, for the control (left) and transient (right) simulations during Mediterranean droughts in 850 – 1849 AD. Black dots on the composites of the transient simulation indicate the regions where the means between the control and transient simulations are statistically not significant at 5% confidence level.

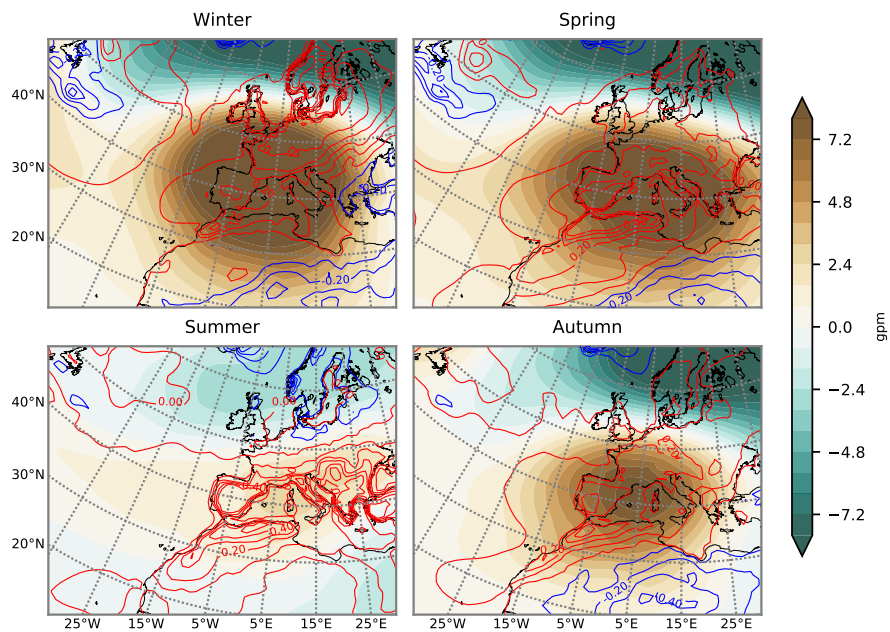


**Figure 8.** Mean geopotential height anomaly at 850 hpa (color shaded) and surface temperature anomaly (contours every  $0.2^{\circ}\text{C}$ , positive in red and negative in blue) during Mediterranean droughts for each season in the transient simulation.

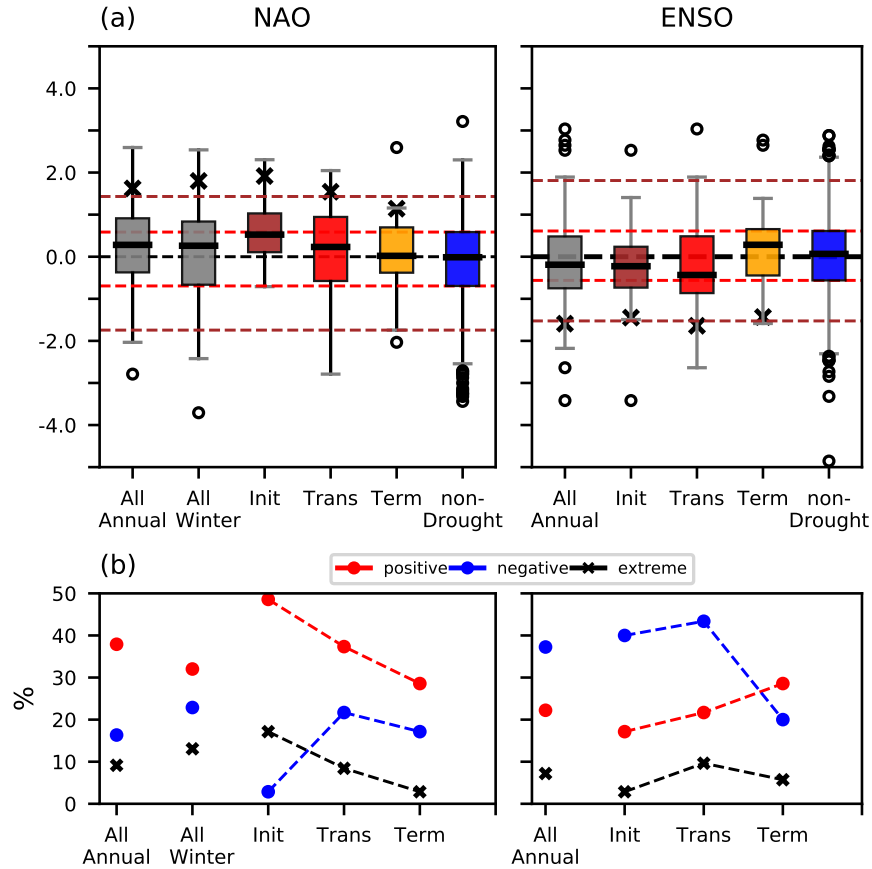


**Figure 9.** (a) Box plots of NAO and ENSO during multi-year Mediterranean droughts. The black crosses indicate 95 percentile value for NAO, and 5 percentile value for ENSO. Dashed red lines indicate the 25 and 75 percentiles of non-drought periods, which are the thresholds to discern negative/positive states of NAO and ENSO. Dashed brown lines indicate 5 and 95 percentile of non-drought periods. (b) Frequencies of occurrences of positive and negative states of NAO (left) and ENSO (right) for annual and winter total, and each stage of droughts. Black crosses indicate the frequencies of occurrence of extreme positive NAO and extreme negative ENSO.

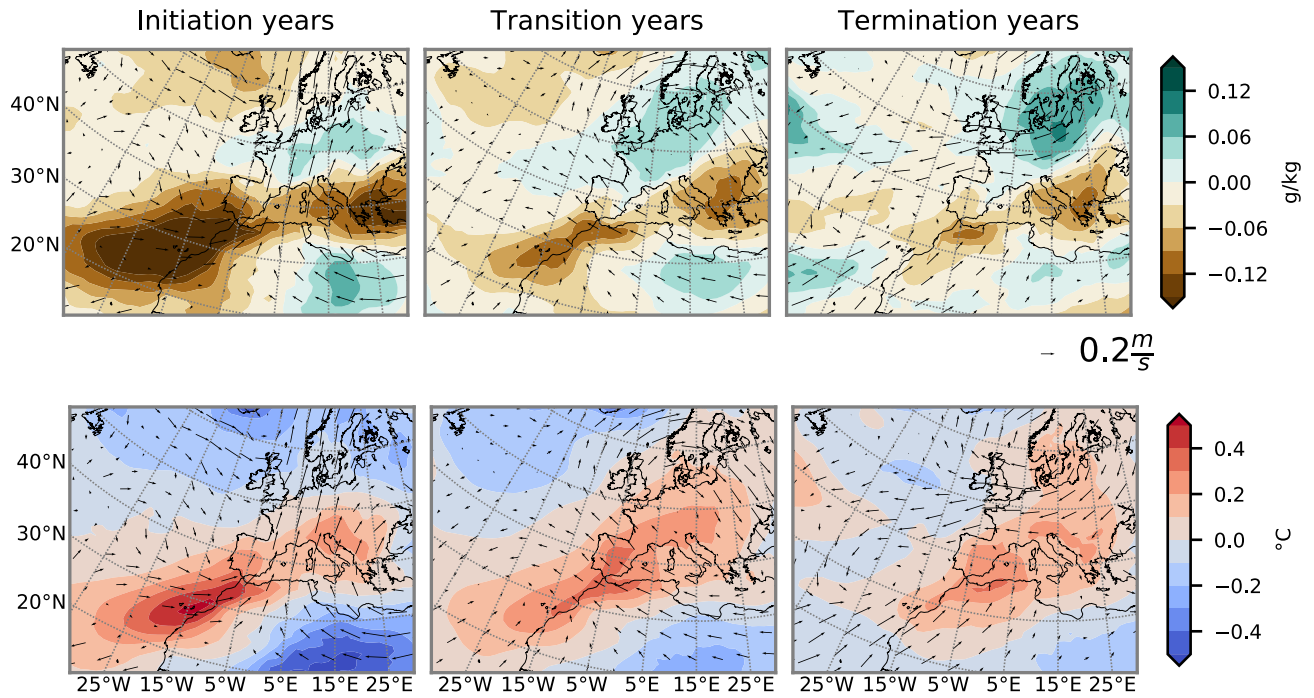


**Figure 10.** Evolution of atmospheric conditions in each stages of droughts. Anomalies of (above) specific humidity, and (below) temperature, both at 925 hPa during initiation, transition and termination years. Arrows indicate winds at 925 hPa.

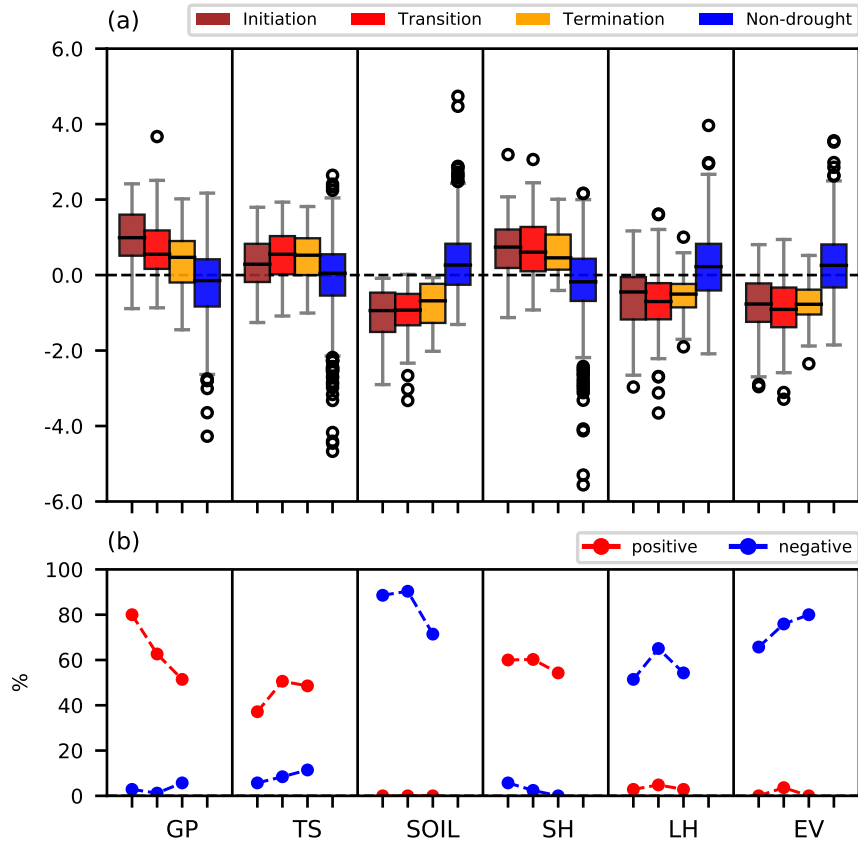


**Figure 11.** Same boxplot as Fig. 9 but for standardized regional atmospheric and soil variables over the region of study during Mediterranean droughts: anomalies of geopotential height at 850 hPa (GP), surface temperature (TS), soil moisture (SOIL), sensible heat flux (SH), latent heat flux (LH) and evapotranspiration (EV). (b) Frequencies of occurrences of positive and negative anomalies in each stage of droughts in order: initiation, transient and termination years.

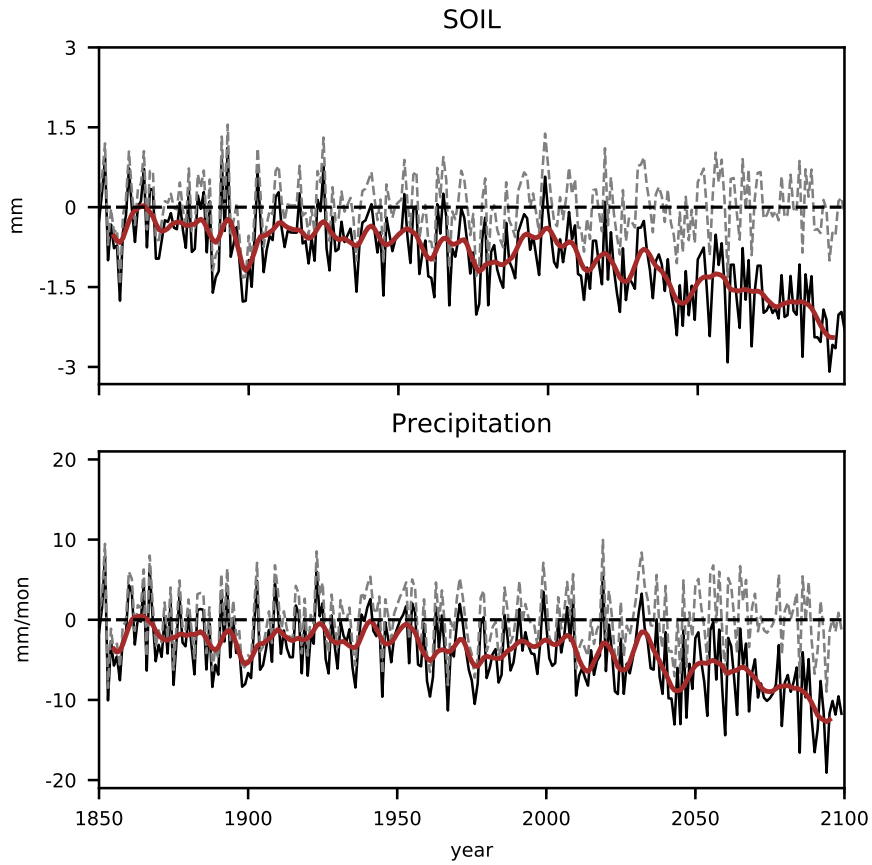


**Figure 12.** Time series of annual soil moisture (SOIL), and precipitation anomalies from 1850 to 2099 AD with respect to the 1000 - 1849 AD means. Brown lines indicate smoothed 10 years running mean, and dashed lines the detrended time series.

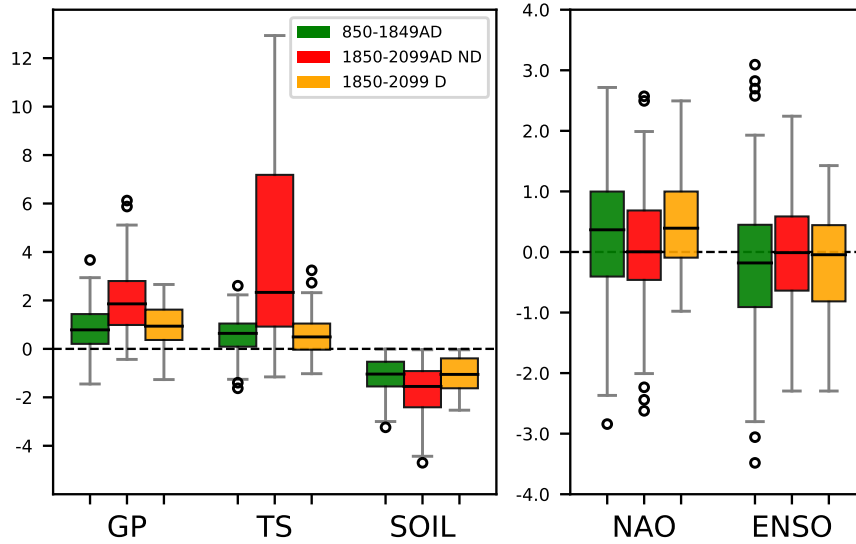


**Figure 13.** (a) Standardized regional variables: anomalies of geopotential height at 850 hPa (GP), surface temperature (TS) and soil moisture (SOIL) over the region of study, and (b) indices of large scale circulation patterns: NAO and ENSO during Mediterranean droughts for the period of 850 - 1849 AD (green), non-detrended 1850 - 2099 AD (red) and detrended 1850 - 2099 AD (yellow). The GP, TS and SOIL between the detrended 1850 – 2099 AD and the 850 – 1849 AD periods present p-values from Mann-Whitney U test of 0.09, 0.02 and 0.29, respectively. For NAO and ENSO, the p-values are 0.19 and 0.29 for each.

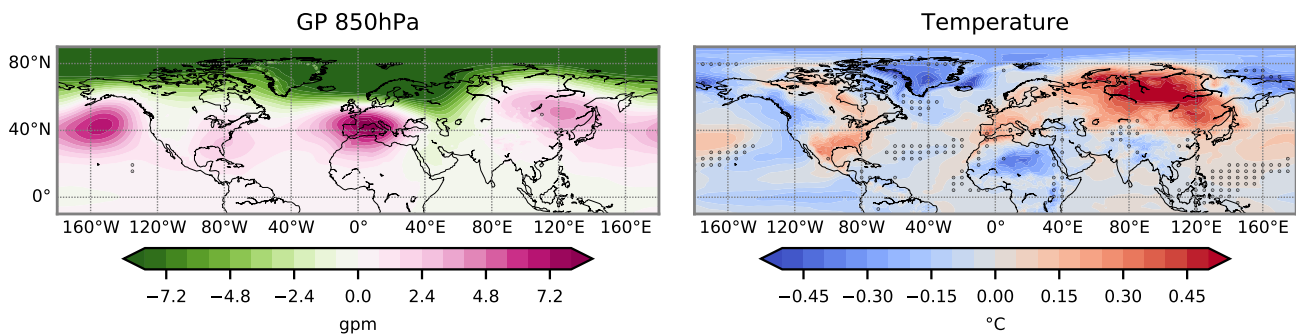


**Figure 14.** Detrended mean geopotential height anomaly at 850 hpa and surface temperature anomaly during Mediterranean droughts for the 1850 - 2099 AD. Black dots indicate the regions where the means between the detrended 1850 – 2099 AD and 850 – 1849 AD are statistically not significant at 5% confidence level (Fig. 7).